

Comparing Dawn, Hubble Space Telescope, and Ground-Based Interpretations of (4) Vesta

Vishnu Reddy

Max Planck Institute for Solar System Research, Katlenburg-Lindau, Germany

Department of Space Studies, University of North Dakota, Grand Forks, USA

Planetary Science Institute, Tucson, AZ 85719, USA

Email: redsky@psi.edu

Jian-Yang Li

Planetary Science Institute, Tucson, AZ 85719, USA

Lucille Le Corre

Planetary Science Institute, Tucson, AZ 85719, USA

Max Planck Institute for Solar System Research, Katlenburg-Lindau, Germany

Jennifer E. C. Scully

Institute of Geophysics and Planetary Physics, University of California Los Angeles, Los Angeles
California, USA

Robert Gaskell

Planetary Science Institute, Tucson, Arizona, USA

Christopher T. Russell

Institute of Geophysics and Planetary Physics, University of California Los Angeles, Los Angeles
California, USA

Ryan S. Park

Jet Propulsion Laboratory, California Institute of Technology, Pasadena, California, USA

Andreas Nathues

Max Planck Institute for Solar System Research, Katlenburg-Lindau, Germany

Carol Raymond

Jet Propulsion Laboratory, California Institute of Technology, Pasadena, California, USA

Michael J. Gaffey

Department of Space Studies, University of North Dakota, Grand Forks, USA

Holger Sierks

Max Planck Institute for Solar System Research, Katlenburg-Lindau, Germany

Kris J. Becker

Astrogeology Science Center, U.S. Geological Survey, Flagstaff, Arizona, USA

Lucy A. McFadden

NASA Goddard Spaceflight Center, Greenbelt, Maryland, USA

51 Figures: 9

52 Tables: 5

53

54 **Proposed Running Head:** Dawn, HST, Ground-based Studies of Vesta

55

56 **Editorial correspondence to:**

57 Vishnu Reddy

58 59-495 Hoalike Road

59 Haleiwa

60 Hawaii 96712

61 (808) 342-8932 (voice)

62 reddy@psi.edu

63

64

65

66

67

68

69

70

71

72

73

74

75

76

77

78

79

Abstract

Observations of asteroid (4) Vesta by NASA's Dawn spacecraft are interesting because its surface has the largest range of albedo, color and composition of any other asteroid visited by spacecraft to date. These hemispherical and rotational variations in surface brightness and composition have been attributed to impact processes since Vesta's formation. Prior to Dawn's arrival at Vesta, its surface properties were the focus of intense telescopic investigations for nearly a hundred years. Ground-based photometric and spectroscopic observations first revealed these variations followed later by those using Hubble Space Telescope (HST). Here we compare interpretations of Vesta's rotation period, pole, albedo, topographic, color, and compositional properties from ground-based telescopes and HST with those from Dawn. Our goal is to provide ground truth for prior interpretations and help identify the limits of ground-based studies of asteroids in general. The improved rotational period measurement from Dawn is 0.222588652 day (Russell et al., 2012), and is consistent with the best ground-based rotation period of 0.22258874 day (Drummond et al., 1998). The pole position for Vesta determined by Dawn is $309.03^\circ \pm 0.01^\circ$, $42.23^\circ \pm 0.01^\circ$ and is within the uncertainties of pole orientation determined by Earth-based measurements (Li et al., 2011: $305.8^\circ \pm 3.1^\circ$, $41.4^\circ \pm 1.5^\circ$). Similarly, the obliquity of Vesta is 27.46° based on the pole measurement from Dawn and all previous pole measurements put the obliquity within 3° of this value. Topography range from Dawn shape model is between -22.45 to +19.48 km relative to a 285 km x 285 km x 229 km ellipsoid. The HST range is slightly smaller (-12 km to +12 km relative to a 289 km x 280 km x 229 km ellipsoid) than Dawn, likely due to lower spatial resolution of the former. We also present HST and Dawn albedo and color maps

of Vesta in the Claudia (used by the Dawn team) and IAU coordinate systems. These maps serve to orient observers and identify compositional and albedo features from prior studies. We have linked several albedo features identified on HST maps to morphological features on Vesta using Dawn Framing Camera data. Rotational spectral variations observed from ground-based studies are also consistent with those observed by Dawn. While the interpretation of some of these features was tenuous from past data, the interpretations were reasonable given the limitations set by spatial resolution and our knowledge of Vesta and HED meteorites at that time. Our analysis shows that ground-based and HST observations are critical for our understanding of small bodies and provide valuable support for ongoing and future spacecraft missions.

1. Introduction

Vesta is one of the most frequently observed objects in the Main Asteroid Belt since its discovery by Heinrich Olbers in 1807. Ground-based color observations of Vesta as early as 1929 (Bobrovnikoff, 1929) revealed surface albedo/color variations that were attributed to composition. Taylor (1973) noted that Vesta's lightcurve changed depending on viewing geometry with northern hemisphere and equatorial views showing a single maximum. Degewij (1978) used polarimetry to verify that Vesta's lightcurve is dominated by albedo. The relationship between albedo and polarization and the overlap with the visual wavelength lightcurve suggested that the observed light curve was indeed controlled by albedo variation. Later photometric observations confirmed that hemispherical scale albedo variations dominate the lightcurve rather than shape (Drummond et al. 1988).

Disk-integrated visible wavelength (0.3 to 1.1 μm) spectral observations of Vesta (McCord et al. 1970) revealed a deep absorption band at 0.9 μm attributed to the mineral pyroxene. Overall spectral shape, and the presence of this pyroxene band, suggested a compositional link between Vesta and the howardites-eucrites-diogenites (HED) meteorites and suggested Vesta as a differentiated object. Rotationally resolved near-IR spectra of Vesta from NASA IRTF suggested that albedo variations might be linked to surface compositional heterogeneity (e.g., Gaffey, 1997; Vernazza et al. 2005; Reddy et al. 2010). Subsequent Hubble Space Telescope (HST) observations confirmed the affinity between compositional variations and albedo units thought to be surface morphological features (Thomas et al. 1997a; Binzel et al. 1997; Li et al. 2010).

149 The Dawn spacecraft entered orbit around Vesta in July 2011 to begin its
150 yearlong mapping mission (Russell et al. 2012). During this period, the spacecraft
151 mapped the surface of Vesta using its three instruments: Framing Cameras (FC), Visible
152 and Infrared Mapping Spectrometer (VIR), and Gamma Ray and Neutron Detector
153 GRaND). The Dawn Framing Cameras (FC) are a pair of identical 1024x1024 pixel
154 imagers equipped with seven color filters (0.44-0.98 μm) and one panchromatic filter
155 (Sierks et al. 2011) that imaged the surface of Vesta with an angular resolution of 93
156 $\mu\text{rad/pixel}$. Only FC2 was used during Vesta mapping phase with FC1 being a backup.
157 Table 1 shows the list of filters along with their central wavelength and band pass. The
158 FC mapped the surface at varying spatial resolution depending on the orbital phase.
159 During approach, three rotational characterization (RC) phases imaged the entire visible
160 surface at 9.07 km/pixel (RC1), 3.38 km/pixel (RC2), and ~ 487 meters/pixel (RC3,
161 RC3B) (Table 2).

162 Dawn is the first mission to an asteroid that has been profusely studied by ground-
163 based telescopes and HST over many decades. This wealth of knowledge not only helped
164 us understand Vesta prior to arrival of Dawn, but also enabled us to verify the validity of
165 these studies. With over 600,000 asteroids discovered so far, and the ever-increasing cost
166 of robotic exploration of small bodies, sending a spacecraft to many of these asteroids is
167 inconceivable. Dawn presents a unique opportunity to verify and validate ground-based
168 observations of Vesta. In this work we aim to compare ground-based and HST data of
169 Vesta with those from Dawn FC to verify interpretations of albedo units and rotational
170 variations. We also provide maps in three coordinate systems: the original Olbers system
171 based on Thomas et al. (1997a); the Claudia system based on Russell et al. (2012) and

used by the Dawn science team; and the IAU coordinate system in which all the Dawn data will be archived on the Planetary Data System (PDS).

2. Data Sets and Processing

Three data sets were used in this paper: ground-based spectral data from Gaffey (1997) and Reddy et al. (2010); HST data from Thomas et al. (1997a), Binzel et al. (1997), and Li et al. (2010); and Dawn FC data from RC1, RC2 and RC3. The best resolution of HST data (38 km/pixel) is compared to the lowest resolution from Dawn during RC1 (9 km/pixel). Data reduction procedures for ground-based data are described in Gaffey (1997), Reddy et al. (2010); and for HST data processing in Thomas et al. (1997a), Binzel et al., (1997) and Li et al. (2010). A detailed description of Dawn FC data processing pipeline is presented in the supplementary materials section of Reddy et al. (2012a). Here we describe processing after the creation of photometrically and spectrally calibrated seven color global mosaics.

HST observations of Vesta at shorter wavelengths show higher contrast in albedo but this is below the wavelength range of Dawn FC filters. The Dawn albedo maps were created by using the 0.75- μm filter data which shows greatest albedo contrast among the FC filters and also has least amount of infield stray light residuals after correction (Reddy et al. 2012a). A global 0.75- μm -filter mosaic was extracted from the seven-color mosaic using IDL ENVI.

In addition to the albedo map, we created a band depth map, and a eucrite-diogenite (ED) ratio map. The band depth map (0.75/0.92 μm) is a single band color-coded map that helps to quantify the 0.9- μm -pyroxene band depth. The ED ratio is an interpretive scheme consisting of a single band rainbow color-coded map that uses the

ratio of 0.98 μm and 0.92 μm filters. Diogenite-rich areas are in red and show a deeper 0.90- μm pyroxene band whereas eucrite-rich areas are in blue (Reddy et al. 2012a). Due to higher iron content in eucrites their 0.9- μm pyroxene band is shifted to longer wavelength and so the eucrite ED ratio is ~ 1 . In contrast diogenites have ED ratio > 1 due to their lower iron abundance (Reddy et al. 2012a).

3. Evolution of Coordinate Systems

The evolution of coordinate systems used on Vesta has historically depended on the spatial resolution of data available at that time (Gaffey, 1997; Thomas et al. 1997b; Russell et al. 2012). Typically, ground-based rotational spectral studies of asteroids (e.g., Reddy et al. 2010) used a lightcurve-based coordinate system where near-simultaneous lightcurve observations are used to phase spectral observations (arbitrarily) with the minima of the lightcurve becoming the prime meridian. Gaffey (1997) observed several distinct compositional units on the surface of Vesta based on rotational spectral observations. Creating a simple compositional map, Gaffey (1997) centered his prime meridian on a compositional unit informally called “Leslie Formation,” which was interpreted as olivine-rich. This corresponds approximately to a weak inflection in brightness around the lightcurve maxima of Vesta (0.75 rotational phase in Fig. 3 of Gaffey 1997). It is important to note that the original maps published in Gaffey (1997) had an error in latitude range. The correct latitude range of Gaffey (1997) maps is 90°N to 60°S .

The general conventions for defining a body fixed coordinate system for Solar System small bodies as adopted by the IAU/WGCCRE are summarized in Archinal et al. (2010). Vesta is in simple rotation with slow precession (Asmar, pers. comm). For this

case, its body fixed coordinate system follows the right-hand rule that defines a “positive pole” by its direction of angular momentum, and the longitude increases towards the direction of rotation. The positive pole of Vesta is above (or on the north of) the invariable plane of the Solar System (prograde rotation), similar to many planets, further simplifying the case without causing any confusion. Using the geodesy conventions, the positive pole of Vesta is thereby always referred to as the “North pole”, and the direction of rotation is referred to as “East”. All coordinate systems defined for Vesta in this work follow these conventions. In addition, when displaying maps, we adopted the convention to position the prime meridian at the center of the map, and longitude running between 0 and 360 (positive values). We adopted one single coordinate system and one single convention for all the maps and figures used here to avoid further confusion.

Historically, Gaffey (1997), Thomas et al. (1997a), and Binzel et al. (1997) maps were produced before the current conventions were adopted, and used a longitude system that increases towards the opposite direction of rotation, i.e., towards west, or a mixed east and west longitude to keep longitude values positive between 0° and 180° in the case of Thomas et al. But except for the longitude system, all those maps were displayed in a compatible orientation with the IAU conventions, i.e., 0-longitude center with north up. In addition, the map generated by Gaffey (1997) used incorrect range of latitude, while his north-south and east-west directions were compatible with the IAU conventions. The maps generated by Li et al. (2010) fully comply with the IAU conventions.

Thomas et al. (1997b) proposed a coordinate system for Vesta based on the rotational axis they derived from HST images and a new prime meridian centered on “the most prominent visible feature.” This prominent feature was a 200 km wide low albedo

unit, which was the largest and most distinct visible feature on Vesta, and was informally called “Olbers Regio” (Zellner et al. 1997) in honor of Vesta’s discoverer Wilhelm Olbers. To calculate the location of the “Olbers” prime meridian for subsequent observations they developed a simple equation that used a rotation period of 0.2225887 day derived by Drummond et al. (1988). All subsequent publications (e.g., Binzel et al., 1997; Vernazza et al. 2005; Zellner et al. 2005; Carry et al. 2010; Li et al. 2010; Reddy et al., 2010, 2012b) till the arrival of Dawn at Vesta used the Thomas et al. (1997b) Olbers coordinate system with the Thomas et al. (1997b) pole measurement. Table 3 shows the values in pre-Dawn coordinate systems and in the Dawn coordinate system for the right ascension (α_0) and declination (δ_0) of the spin pole of Vesta and for the ephemeris position of the prime meridians. Binzel et al. (1997) updated the Vesta lithologic map from Gaffey (1997) into the Olbers coordinate system, and found that the prime meridian in Gaffey’s maps was at $\sim 255^\circ$ east of Olbers.

Early in Dawn’s encounter with Vesta the Dawn science team derived a coordinate system that was founded upon the new spacecraft-derived knowledge of the asteroid’s surface. The system is defined by Claudia crater, which is a ~ 625 meter diameter crater located in Vesta’s Oppia quadrangle (Russell et al. 2012). The location of the crater center is 1.6°S , 356.0°E in Claudia system coordinates. Vesta’s prime meridian is 4° east of Claudia’s position. Longitude increases to the east of the prime meridian. The Dawn team has undertaken all mapping and science investigations in the Claudia coordinate system.

The purpose of the Claudia coordinate system is to provide a convenient framework for representing and navigating the surface of Vesta, which is in accordance

with the observations made by the Dawn spacecraft. Consistent with IAU best practices the Dawn Science team chose a small crater near the equator to anchor the coordinate system. The prime meridian was located for the convenience of the mappers, whose quadrangles are aligned with the prime meridian. It is traditional in mapping planetary surfaces to have the quadrangles all begin aligned with the prime meridian. The choice of the Dawn coordinates ensured that. No significant features were split by the prime meridian. Further, the prominent ‘Snowman’ craters, Marcia, Calpurnia and Minucia, were centrally located. It was believed to be safer for the users of the Dawn observations to work with a unique coordinate system that is clearly distinct from the early coordinate systems, which are based on various pole locations. These earlier coordinate systems (Li et al., 2011; Archinal et al., 2011; Seidelmann et al., 2007; Seidelmann et al., 2005; Seidelmann et al., 2002; Thomas et al., 1997) are nearer to the 180° meridian of the Claudia coordinate system. With the large difference between the Claudia system and the earlier systems, the use of the Claudia coordinate system can be easily visually verified. In practice, this choice of coordinate systems enabled those operating the spacecraft, and processing the data to spot errors by visual inspection. Coordinate system errors were not uncommon, but were found promptly with this device (S. Joy, personal comm., 2011).

Claudia was chosen out of the innumerable small craters in the general location of the prime meridian, first because according to standard practices, it is close to the equator. Also it can be simply located by the use of a number of marker craters. Claudia is located roughly midway between Oppia and Gegania craters and to the north of Divalia Fossa. Claudia and eight larger craters form a cursive uppercase H (dotted lines in Fig. 1a), in which Claudia lies on the bar of the H. Near the midpoint of this bar are two

craters that are merged together and have a small crater in the center of their eastern rim (see Fig. 1b). Claudia is roughly 3.5 kilometers to the southeast of this small crater. Claudia was also chosen because it has a distinctive morphology, which makes it distinguishable from other similarly sized craters (see Fig. 1c). Claudia has a sharp, fresh rim; there is a ~170 meter diameter crater on the northeastern rim and two ~80 meter craters, along with many smaller craters, within Claudia's interior.

4. Comparison of Rotational Period and Pole Orientation

All early determinations of the rotational period of Vesta were performed through its rotational lightcurves (e.g., Cuffey, 1953; Groeneveld and Kuiper, 1954; Gehrels, 1967; Taylor, 1973; Chang and Change, 1962; Haupt, 1958; Magnusson, 1986). Although the rotational period of Vesta has been determined to an accuracy of 10^{-7} days, there was an ambiguity of whether Vesta's rotational period is 5.34 hr or 10.68 hr, rising from whether its lightcurve is single-peaked or double-peaked. Later observations using polarimetry, speckle interferometry, and radar favored the shorter period and showed that the surface of Vesta is variegated possibly due to compositional heterogeneity (Degewij et al., 1979; Drummond et al., 1988; Taylor et al., 1985). With the help from speckle interferometry and adaptive optics (AO), the surface of Vesta was resolved and the lightcurve of Vesta is shown to be single-peaked (Drummond et al., 1988). Using a large dataset of AO images, Drummond et al. (1998) determined a rotational period of 0.22258874 day with an uncertainty of 4 on the last decimal place (3.5 ms). This is the most accurate determination of Vesta's rotational period before Dawn's arrival at Vesta. The improved rotational period measurement from Dawn is 0.222588652 day with an uncertainty of 35 μ s (Russell et al., 2012).

The pole orientation of Vesta was previously determined from ground-based and HST observations before Dawn arrived at Vesta with different datasets and techniques (Table 3). Thomas et al. (1997a) used HST images acquired in 1994 and 1996 with pixel sizes of 54 km and 38 km at Vesta, respectively, to construct a shape model of Vesta and determine its pole orientation based on surface albedo features and the limb profiles of the disk. They reported a pole orientation of (RA=301°, Dec=41°) with an uncertainty of 10° on both RA and Dec. Drummond and Christou (2008) fitted an ellipsoidal model to the limb of observed disk of Vesta from various observing and illumination conditions using ground-based, disk-resolved observations with speckle interferometry and adaptive optics techniques over the past 27 years. Their best-fit pole orientation was (306°, 38°) with an uncertainty of 7°. Li et al. (2011) combined all previous determinations of Vesta's pole orientation and their newly acquired images from HST in 2007 and 2010 at similar pixel size of previous HST images. They experimented with two methods, namely control point stereogrammetry and feature tracking, on all four HST datasets combined, and performed statistical studies of previous pole determination with ground-based data. The latest measurement of Vesta's pole orientation before Dawn measurements was (305.8°, 41.4°)±(3.1°, 1.5°) by Li et al (2011). While in orbit around Vesta, the Dawn spacecraft returned a substantial amount of imaging and tracking data, which have been used to precisely determine the pole orientation of Vesta as (309.03°, 42.23°) with an uncertainty of 0.01° (Russell et al., 2012). The obliquity of Vesta is 27.46° based on the pole measurement from Dawn. All previous pole measurements put the obliquity within 3° of this value (Table 3).

5. Comparisons between HST and Dawn FC lightcurves

333 HST observed Vesta four times in 1994 (Zellner et al., 1996), 1996 (Thomas et al.,
334 1997b), 2007 (Li et al., 2010), and 2010 (Li et al., 2011), all with WFPC2 through the
335 same set of filters; F439W, F673N, F953N, and F1042M. While the observing
336 circumstances were all different, the 2007 observations have a sub-solar latitude of -5.3° ,
337 being the closest to the sub-solar latitude of Dawn data collected while approaching
338 Vesta (south of -23°) among all HST observations. To compare the whole-disk
339 lightcurves of Vesta collected by Dawn FC with those obtained by HST, we focus on
340 HST 2007 observations and FC images collected on June 30, 2011 that cover one full
341 rotation of Vesta. The observing geometries of both observations are listed in Table 4.

342 The shape of Vesta is close to a tri-axial ellipsoid, with the short axis aligned to
343 its rotational axis. The difference between its intermediate axis and long axis is less than
344 3% (Thomas et al., 1997b; Russell et al., 2012). The rotational lightcurve of Vesta is
345 single-peaked, and dominated by the albedo variations on its surface rather than by cross-
346 sectional area variation or scattering geometry variation from global-scale topography.
347 Due to moderate multiple scattering on Vesta (Li et al., 2012), the limb-darkening effect
348 is stronger on Vesta than that on darker objects such as the Moon and C-type asteroids.
349 Therefore albedo features near sub-solar point contribute slightly more to the shape of its
350 lightcurve than those near the limb or terminator. For this reason, we plotted the
351 brightness of Vesta with respect to sub-solar longitude rather than sub-observer longitude
352 to compare the lightcurves obtained at different geometries. This is especially necessary
353 for our case because the Dawn FC imaged the morning side of Vesta, while HST imaged
354 the slightly afternoon side of Vesta, and the phase angles of both observations are quite
355 different (Table 4).

Fig. 2 shows the lightcurves of Vesta measured from HST images (green) and Dawn FC images (red and orange). At all three wavelengths, the overall agreement between two observations is excellent in terms of the shape, amplitude, and phase of lightcurves. The Dawn FC lightcurve is much smoother than the HST lightcurve, presumably due to much higher signal-to-noise ratio in Dawn FC images measurement where Vesta is resolved to 9.2 km/pix, compared to 38 km/pix in 2007 HST images. The slight difference at sub-solar longitude from 60° to 330° could be due to viewing angle difference. Dawn images have much more southern latitude than that of HST images, and in mid northern latitude (30°-60°) the surface of Vesta appears to be brighter in this range of longitude than in other longitudes.

Compared to the albedo maps (Fig. 4), the large bright and dark features in the lightcurves (Fig. 2) all correspond to the large-scale albedo features. The lightcurve minimum is located between longitude 270° and 330°, corresponding to the broad dark area on Vesta observed in the same longitude. The lightcurve maximum is located between longitude 60° to 120°, when the bright eastern hemisphere is visible. Compared to the lightcurve minimum, the lightcurve peak appears to be slightly round-shaped or plateaued. This is due to the large, relatively dark area near Oppia near ~100° longitude surrounded by broad bright areas.

6. Comparison of Vesta shape model from HST and Dawn

The topography of Vesta was constructed using the technique of Gaskell et al. (2008) from over 150000 small 99x99 pixel maplets, each representing the topography and relative albedo of a small patch of Vesta's surface. Each maplet is located in an image by illuminating its topography under the same viewing conditions as the image and

performing a simple correlation. The center of the maplet represents a control point in image space, and due to the maplet's three-dimensional structure, its control point can be located in many images in a wide range of illuminations, resolutions and viewing geometries. This leads to an extremely precise solution for the location of the maplet's center. Similarly, the positions of many control points in a single image yield a precise determination of the Vesta-relative camera position and pointing at the image time (Gaskell, 2011). The maplets themselves are constructed by adjusting the slope and relative albedo at each of its pixels to minimize the residuals between the image brightness and illuminated maplet pixel brightness over a large number of images. The slopes are then integrated to produce the topography distribution within the maplet.

The ensemble of maplets can be combined to produce a global topography for Vesta's surface (Gaskell, 2012, private communication). Figure 3B shows this topography in a frame very close to the original Thomas et al. (1997a) coordinate system. The heights range from -22.45 km (blue/violet) to +19.48 km (red) relative to a 285 km x 285 km x 229 km ellipsoid. Thomas et al. (1997a) were able to glean the topography of Vesta from images gathered by the Hubble Space Telescope. Their map, relative to a 289 km x 280 km x 229 km ellipsoid is shown in Figure 3A. There are striking similarities between the Thomas Hubble topography and the Dawn determined results. The Thomas range of heights was slightly smaller, but in general the agreement is very good and the differences can be explained in part by the dramatic difference in resolution between the two data sets.

Thomas et al. (1997a) note that the south pole (now called Rheasilvia) basin has a diameter of 460 km with an average depth below the rim of 13 km. The central peak

within the basin is 13 km high compared to its deepest parts in HST map (Thomas et al. 1997a). In comparison, Dawn data show that the basin has a diameter of $\sim 500 \pm 25$ km and a depth of 19 ± 6 km (Schenk et al. 2012). While these values are greater, they are consistent with HST model given the resolution of the data and the reference ellipsoids used. Thomas et al. (1997a) also note that a small section of the Rheasilvia rim is ~ 5 km higher than other parts. This region corresponds to Matronalia Rupes in Dawn data and rises higher than the rest of the basin rim as observed in HST data (Schenk et al. 2012).

7. Comparison of HST Observations and Dawn FC Data

7.1 Global View

Figure 4a shows the HST map of Vesta in 0.673- μ m filter projected in the Thomas et al. (1997a) coordinate system based on observations from 1994, 1996 and 2007 oppositions at a resolution of ~ 50 km/pixel. The prime meridian here is defined through the dark feature informally named “Olbers” in Thomas et al. (1997a) located at $\sim 15^\circ$ N. The pole position for this data is $\alpha_0 = 301^\circ \pm 5^\circ$, $\delta_0 = 41^\circ \pm 5^\circ$. Figure 4b shows the Dawn FC map of Vesta in 0.75- μ m filter from RC1 at a resolution of 9.06 km/pixel with the prime meridian similar to Thomas et al. (1997a) coordinate system in Fig. 4a. The pole position ($\alpha_0 = 309.03^\circ \pm 0.01^\circ$, $42.23^\circ \pm 0.01^\circ$) is the updated one from Russell et al. (2012) and hence features in the Dawn FC map are slightly rotated with respect to HST map. The Dawn data does not extend to northern latitudes in this map because of the spacecraft location with respect to Vesta during the RC1 phase. Fig. 4c is similar to Fig. 4b but the prime meridian is defined in the Claudia coordinate system (Russell et al. 2012) used by the Dawn science team in all their publications. The purpose of these three figures is to help ground-based observers orient themselves to features on Vesta from Dawn data.

7.2 East-West Dichotomy

Figure 4A-C also helps identify several hemispherical scale albedo features first observed in HST data by Thomas et al. (1997a). Despite the differences in pole position between Figures 4a and 4b, the Western hemisphere has an overall lower albedo than the Eastern hemisphere. Based on rotationally resolved near-IR spectra, Gaffey (1997) suggested that the dark hemisphere could be a howardite or polymict eucrite regolith that has been darkened by ‘age-related darkening effect.’ Binzel et al. (1997) was the first to detect this East-West dichotomy from HST images and interpreted the Western hemisphere as being “dominated by iron-rich and relatively calcium-rich pyroxene” similar to basaltic flows like eucrites. Zellner et al. (2005) suggested albedo features on Vesta could be impact craters/basins filled with dark material similar to lunar mare. Near-IR observations obtained by Vernazza et al. (2005) indicated that the Western hemisphere could be dominated by eucrite-type material. More recently, HST observations by Li et al. (2010) showed that this hemisphere is predominantly a large eucritic unit using the band ratio relationships associated with spectral characteristics of HED meteorites. Using ground-based spectral observations, Reddy et al. (2010) concluded that the Western hemisphere is dominated by howardite/polymict eucrite. Li et al. (2010) and Reddy et al. (2010) observations were also made at southerly sub-Earth latitude (-18.9°) compared to previous studies (16°) (Gaffey 1997 and Binzel et al. 1997).

Reddy et al. (2012a) studied the albedo and color variations on Vesta using Dawn FC color images. These albedo/color maps are in excellent agreement with HST albedo maps from Binzel et al. (1997) and Li et al. (2010) at hemispherical scale (Fig. 5 and 6). Interpreting the composition of the Western hemisphere, they concluded that it is

dominated by a howardite and/or polymict eucrite, which is in agreement with ground-based (Gaffey, 1997; Vernazza et al. 2005) and HST observations (Binzel et al. 1997). However, Reddy et al. (2012a and 2012b) conclude that the cause of the lower albedo in the Western Hemisphere is not due to an age darkening effect (Binzel et al. 1997) or lunar mare type material filling impact craters/basins (Zellner et al. 2005) but due to the in fall of carbonaceous chondritic material. The presence of exogenous carbonaceous chondrite meteorite clasts in some howardite-eucrite-diogenite (HED) meteorites from Vesta is well documented (e.g., Buchanan et al., 1993; Zolensky et al., 1996). In HEDs, carbonaceous chondrite clasts generally make up to 5 vol. % (Zolensky et al., 1996), but on rare occasions can be 60 vol. % of howardites (Herrin et al. 2011). While some of these clasts have been heated and dehydrated during impact ($\sim 400^{\circ}\text{C}$), a majority of them are still hydrated (containing H_2O^- and/or OH^- bearing phases) (Zolensky et al., 1996). Carbonaceous chondrite clasts are the largest exogenic material observed in HED meteorites, but surprisingly they were not suggested as analogs for the dark hemisphere on Vesta by most ground-based and HST studies. Ground-based telescopic observations of Vesta in the mid-IR indicated the possible presence of a $3\text{-}\mu\text{m}$ absorption feature (Hasegawa et al. 2003). Hasegawa et al. (2003) noting the presence of a $3\text{-}\mu\text{m}$ absorption suggested contamination from impacting carbonaceous chondrites as possible cause of this feature.

Rivkin et al. (2006) observations did not find the same feature reported in Hasegawa et al. however, the 2006 observations were at a different viewing geometry than 2003 and did not extend as far North as 2003, and variability of spatial extent of the $3\text{-}\mu\text{m}$ feature was offered as a possible explanation. A weak absorption band at $2.8\text{ }\mu\text{m}$

471 attributed to OH adsorption is reported with variable expression in the spatial domain
472 (DeSanctis et al., 2012b). Evidence of hydrogen enrichment in the same region has been
473 found by Dawn (Prettyman et al. 2012) and confirms the ground-based evidence for a
474 water-related feature near the vibrational bands of hydrated species.

475 Gaffey (1997) and Binzel et al. (1997) interpreted the higher albedo Eastern
476 hemisphere as impact excavated plutonic material similar to diogenites. They also
477 identified several compositionally distinct units using band parameter systematics and
478 concluded that several Eastern hemisphere units have substantial olivine component
479 (more discussion on olivine in Section 6.3). Vernazza et al. (2005) and Carry et al. (2010)
480 also interpreted spectral variations in near-IR to indicate a substantial diogenite in the
481 Eastern hemisphere of Vesta using ground-based spectral and adaptive optics data. Li et
482 al. (2010) and Reddy et al. (2010) concluded there might be a large diogenite unit
483 straddling the boundary between the two hemispheres.

484 Reddy et al. (2012a) mapped the abundance and distribution of diogenite-rich
485 material on Vesta using Dawn FC color images and color indicators of HED components.
486 Albedo (0.75- μm filter), pyroxene band depth (0.75/0.92- μm filter ratio) and eucrite-
487 diogenite (ED) ratio (0.98/0.92- μm filter ratio) maps of Vesta (Fig. 6a-c) from Dawn FC
488 confirm the presence of diogenite-rich material in the southern hemisphere. The ED ratio
489 map shows diogenite-rich areas in red and eucrite-rich areas in blue (Fig. 6c). The
490 distribution of diogenite is predominantly restricted to the southern hemisphere except for
491 a small region that stretches north between 120°-180° W longitude that Reddy et al.
492 (2012a) interpreted as ejecta from the Rheasilvia basin.

493 *7.3 North-South Dichotomy*

Thomas et al. (1997a) studied the southern hemisphere of Vesta using HST. They noted that the band depth and width of the 0.9- μm pyroxene absorption increased with “excavation depth, consistent with exposure of a higher calcium content and coarser grained pyroxene-rich plutonic assemblage within the crust of Vesta or the exposure of olivine present within the upper mantle or both.” Reddy et al. (2010) observed the southern hemisphere of Vesta using the IRTF and concluded from near-IR absorption band position that Vesta’s southern hemisphere is more diogenitic than the northern hemisphere. These conclusions were consistent with Li et al. (2010) HST observations of the Southern hemisphere of Vesta.

The ED ratio map of Vesta produced from Dawn data (Fig. 6c) shows more diogenite-rich material (red) in the southern hemisphere centered around the Rheasilvia basin and bluer eucritic areas in the north confirming ground-based (Gaffey 1997, Reddy et al. 2010) and HST observations (Thomas et al. 1997; Li et al. 2010) of Vesta. There is also a distinct correlation between the albedo (Fig. 6a), band depth map (Fig. 6b), and ED map (Fig. 6c). Brighter areas in the albedo map correspond to areas with deeper band depth and diogenite-rich areas and conversely darker areas correspond to those with weaker band depth and more eucrite-rich areas.

Reddy et al. (2012a) explored the cause of deeper band depth in diogenite-rich areas and concluded that this could be a particle size effect as suggested by Thomas et al. (1997a). Based on meteoritic evidence, the average grain size of diogenites in howardite breccias ranges from 500 μm to 1.5 millimeters whereas the average grain size of eucritic material is $\leq 70 \mu\text{m}$ (Beck and McSween, 2011). This difference could be due to a combination of surface composition and regolith processes (Chamberlain et al. 2007).

Diogenites cooled at depth with coarser (pyroxene) grains compared to eucrites, which are typically fine-grained basalts (surface flows). The larger grain size for diogenites could also be explained by shorter surface exposure ages (fresher impacts) compared to eucrites that might have experienced longer exposures to regolith processes on the surface (impact gardening) (Reddy et al. 2012a). The latter would indicate Rheasilvia basin forming more recently excavating diogenite rich material.

7.4 Cross correlation between HST and Dawn FC Albedo Maps

Binzel et al. (1997) identified 19 different albedo and color units on Vesta using HST observations. These alphabetically ordered units were selected for their spectral diversity that included albedo, band depth, and width (ED). Following similar methods, Li et al. (2010) expanded this list to include 15 new features (numerically ordered) in the southern hemisphere. Of these 34 features identified in HST images, a few are prominently visible in albedo maps while others stand out in band depth and ED ratio maps. Figure 7A shows those units in the albedo map of Vesta from HST in 0.673- μm filter and Fig. 7b shows the same units as identified in the albedo map from Dawn FC in 0.75- μm filter. Both maps are in Thomas et al. (1997a) coordinate system.

Albedo features from the HST map have been identified and labeled on the Dawn FC map by correlating albedo patterns visually and confirming them based on the description of their spectral properties from Binzel et al. (1997) and Li et al. (2010). The most prominent albedo features that are easily identifiable in both maps include low albedo features such as “Olbers,” features #8, #9, A, and B within the dark unit, features Q and #15. High albedo units that are relatively easy to identify in both maps include features #4, #15, #13, #11, and Z. Given the differences in spatial resolution (50 km/pixel

vs. 9 km/pixel) and pole orientation, some diffuse features in the HST map (Fig. 7a) cannot be confirmed in the Dawn FC map shown in Fig. 7b. A complete list of HST units and their corresponding surface features with IAU approved names from Dawn FC images is in Table 5.

7.5 Interpretations of specific features

Ground-based rotationally resolved spectroscopy of Vesta led to the identification of specific compositional units on Vesta (Gaffey, 1997). By correlating variations in spectral parameters (Band Centers and Band Area Ratio or BAR) with rotational lightcurve of Vesta, the location of distinct mineralogical units could be constrained longitudinally and helped create the first maps (Gaffey, 1997). Subsequent disk-resolved color filter observations by HST (Thomas et al. 1997) led to the identification of albedo features associated with these units (Binzel et al. 1997) in the northern hemisphere. Li et al. (2010) identified additional compositional units in the southern hemisphere of Vesta from HST images and Reddy et al. (2010) linked these to specific mineralogical units based on ground-based spectra.

Thomas et al. (1997a) observed three distinct regions that had showed variations in band depth and band width. These include the Rheasilvia basin (discussed in section 6.1), Matronalia Rupes on the rim of the South Pole crater, and a potential crater. Matronalia Rupes feature on Dawn FC maps corresponds to feature #7 (Table 5) on HST maps. This 20-km high scarp (Schenk et al. 2012) stretches for nearly 200 km around the Rheasilvia basin. Thomas et al. (1997a) noted a reverse compositional trend in Matronalia Rupes “consistent with composition of excavated material that has been overturned.” Dawn FC color images show Matronalia Rupes is dominated by diogenite-

rich material (Reddy et al. 2012a) excavated during the formation of the Rheasilvia basin consistent with Thomas et al. (1997a) interpretation. Li et al. (2010) also identified several features (#4, #5, #6) that are interpreted as diogenite-rich areas “located on high rims of the crater.” All these units are located along the rim of the Rheasilvia basin or within the diogenite-rich ejecta blanket that spreads north between 180° and 120°W longitude in Fig 6A-C. This ejecta blanket and diogenite units have also been observed in ground-based compositional map from Gaffey (1997) and Reddy et al. (2010).

Gaffey (1997) noted a decrease in ratio of 2- μ m pyroxene band (Band II) area to that of 1- μ m pyroxene band (Band I) area from ground based spectral observations as Vesta rotated. A well established cause for decrease in BAR is increase in the abundance of olivine in a mixture of olivine and orthopyroxene (Cloutis et al. 1986). Based on this interpretation Gaffey (1997) suggested the presence of a large olivine-rich unit on the surface of Vesta located between 60-120° E longitude (Fig. 8-9). This olivine-rich unit geographically corresponds to feature #15 from HST map of Li et al. (2010) (Fig. 7A-B). This feature has the reddest spectra color over the entire surface of Vesta observed by the HST (Li et al. 2010) with band depth shallower than the background surface.

In Dawn FC color maps (Fig. 6A-C) this feature corresponds to the Oppia crater and its ejecta blanket. Reddy et al. (2012a) observed that Oppia has the reddest visible spectra slope (0.75/0.44 μ m) on Vesta consistent with Li et al. (2010) HST observations. The band depth (0.75/0.92 μ m) of Oppia region is also shallower than the average surface of Vesta (Reddy et al. 2012a). Due to low albedo, red slope and weaker pyroxene bands, Li et al. (2010) interpreted this region to be space weathered (Fig. 8). Investigating the composition of Oppia region, Le Corre et al. (2012) estimated the BAR as 1.57, which is

much lower than the average BAR (2.74) for Vestan surface (Gaffey, 1997). Le Corre et al. (2013) attributed this low BAR to impact melt or excavation of cumulate eucrite layer by the Oppia impact. Hence the low BAR for Oppia region, which was interpreted as olivine by Gaffey (1997), might not be interpreted so today. The best way to determine the presence of olivine on Vesta's surface is through the interpretation of higher resolution data from Dawn. We also rule out selective lunar-style space weathering as the cause of the red visible slope and lower BAR observed in color and spectral data of Oppia (Pieters et al. 2012).

As noted earlier, Zellner et al. (1997) unofficially named a prominent low albedo feature on Vesta as "Olbers Regio" in honor of its discoverer Wilhelm Olbers. This feature also defined the location of the prime meridian in HST maps. Binzel et al. (1997) interpreted this low albedo feature as "remnants of Vesta's ancient basaltic crust." They also noted that the pyroxene band depth of the Olbers feature was relatively shallow and narrow suggesting the predominance of a single pyroxene. Invoking lunar-style space weathering to explain the low albedo and shallow pyroxene absorption band of Olbers, Binzel et al. (1997) concluded that Olbers is remnant ancient crust.

Dawn FC observations of Vesta show that the Olbers region in the HST map corresponds to the dark area East of Marcia, Calpurnia, and Minucia craters. Consistent with HST observations by Binzel et al. (1997) this region has low albedo and weaker pyroxene band compared to Vesta global average. Prettyman et al. (2012) noted an enhancement in hydrogen signature corresponding to Olbers region based on GRaND observations of Vesta and attributed this to the presence of H₂O/OH in carbonaceous chondrite xenoliths. Although our study of this region is still ongoing, the ejecta

distribution around Marcia suggests that it is younger than low albedo region east of it. The low albedo and weaker pyroxene bands of Olbers region are probably due to the mixing of carbonaceous chondrite impactor material and ancient howardite regolith.

One of the brightest albedo spots in HST observations of Vesta is feature #13 from Li et al. (2010). They observed that this feature has an extremely blue spectral slope and is located on the steepest slope(s) on Vesta. The depth of the pyroxene absorption band of this feature is indistinguishable from the background surface in HST observations. In ground based observations of Vesta (Binzel et al. 1997; Gaffey, 1997) this feature corresponds to a diogenite-rich unit located $\sim 45^\circ$ S latitude. In Dawn FC images, this feature corresponds to ejecta around the Antonia crater, a 17.4-km diameter impact feature within the Rheasilvia basin. The Framing Camera shows that Antonia crater is indeed located on a topographically steep slope on Vesta consistent with HST observations by Li et al. (2010). ED ratio map of Vesta (Fig. 6b-c) showed that the region around Antonia crater is dominated by diogenite-rich material consistent with ground-based observations by Gaffey, (1997).

Of the six geologic units identified by Li et al. (2010) in HST images (Fig. 9), area IV (60° E longitude) showed a deep pyroxene band, neutral red slope and was interpreted as diogenite rich. In Dawn FC data (ED map), this region corresponds to 30-km diameter Numisia crater, which lies SE of Olbers region. Numisia has been interpreted as diogenite-rich consistent with HST observations.

7.6 Space Weathering

Space weathering consists of processes by which the surface optical properties are modified when exposed to space environment in the absence of an atmosphere. On the

632 Moon the primary effect of space weathering is decrease in optical albedo, increase in
633 spectral slope (reddening), and a decrease in absorption band depth (Pieters et al. 2000;
634 Taylor et al. 2001). Nano phase iron created during space weathering coats the lunar soil
635 grains causing these observed effects (Loeffler et al. 2008). In contrast to the Moon,
636 asteroids visited by spacecraft prior to the arrival of Dawn at Vesta showed distinctly
637 different effects of space weathering (Gaffey, 2010). On (243) Ida, the band depth
638 decreased and the spectral slope increased, while the albedo remained nearly constant
639 with increased level of space weathering (Veverka et al. 1996). On (433) Eros, the overall
640 albedo decreased but the spectral slope and band depth remained nearly constant with
641 increased level of space weathering (Murchie et al. 2002).

642 Space weathering on Vesta has been a source for intense scrutiny over the last two
643 decades because of its similar basaltic composition as that of the Moon. Detection of
644 large-scale albedo variations on Vesta using HST suggested that some of them might be
645 ancient ‘space weathered’ units (Binzel et al. 1997). Hiroi and Pieters (1998) conducted
646 simulated space weathering experiments on HED meteorites and compared them to Vesta
647 and Vestoids. Vestoids are small asteroids (~10 km) that have spectral properties similar
648 to Vesta and are part of the Vesta dynamical family. They found that Vesta and some
649 Vestoid spectra showed effects similar to lunar style space weathering, but some Vestoid
650 spectra did not follow the “HED-lunar space weathering trend.” They concluded that
651 these Vestoids could be from a different parent body. Addressing the cause of “bluer”
652 visible spectra of Vesta, Vernazza et al. (2006) invoked the possibility of a magnetic field
653 around Vesta that could be protecting the surface against lunar-style space weathering
654 effects. Meteoritical evidence for space weathering products in Vestan regolith has been

limited. Noble et al. (2011) searched for space weathering products (agglutinates and nano phase iron bearing rims) in howardite Kapoeta and found several “melt products, including spherules and agglutinates and possible nano phase bearing rim.” They concluded that the presence of these products would suggest that lunar style space weathering is active on asteroids like Vesta.

Analyzing Dawn FC and VIR spectral data, Pieters et al. (2012) noted that Vesta’s surface shows effects of space weathering but it is unlike that seen on the Moon. They also found no evidence for the accumulation of nano phase iron, which is the principle cause of lunar space weathering effects, on Vesta’s regolith particles. Gradual fading of freshly exposed material seen on Vesta has been attributed to localized mixing of material with diverse spectral and albedo properties (Pieters et al. 2012, McCord et al. 2012, Li et al. 2012). McCord et al. (2012) have shown that impact mixing of bright pristine material (Li et al. 2012) with darker exogenous carbonaceous chondrite material (Reddy et al. 2012) gives rise to the background gray material. In light of this new information from Dawn, it appears that general application of lunar style space weathering to all asteroids is invalid. This result is also consistent with space weathering trends observed on other asteroids by spacecraft (Ida and Eros) that suggest unique styles of space weathering operating on each of these objects (Gaffey, 2010).

8. Future Earth-Based Observations

Studies of Vesta by ground-based and orbiting telescopes helped the Dawn mission to be better prepared to explore Vesta. While the results from the mission has confirmed many pre-Dawn characterizations of Vesta, a myriad of surprises were revealed, which could only be possible with an orbital mission. Based on the comparison of ground-based and

HST data of Vesta with Dawn's Framing Camera data, we can conclude that ground based observations have been extremely accurate at constraining rotation period, surface composition using reflectance spectroscopy, and detecting/mapping rotational spectral variations on small bodies. HST observations have also been successful in accurately identifying albedo and color features, surface composition of these features and constraining the shape, pole orientation and topography. The success of these precursor studies can be attributed to two factors: a) availability of high quality ground-based and HST data, and b) interpretations backed by laboratory studies of HED meteorites that were delivered to Earth from Vesta.

However, ground-based observations and their interpretations have severe limitations in accessing the prevalence and magnitude of space weathering on individual small bodies. As noted earlier, space weathering on Vesta (Pieters et al. 2012) and other small bodies visited by spacecraft has been shown to be unlike that on the Moon (Gaffey, 2010). On Vesta, alternate processes such as presence of exogenous opaques (Reddy et al. 2012b; McCord et al. 2012), observing geometry/phase angle (Reddy et al. 2012c; Sanchez et al. 2012) and particle size (Reddy et al. 2012a; Pieters et al. 2012) have been shown to be the cause of traditional lunar-style space weathering effects like low albedo, red spectral slope, and weaker absorption bands. The effects of multiple impacts from large and small projectiles control the distribution and mixing of materials in Vesta's regolith. Future interpretations of ground-based spectra of small bodies must take into account these findings from Dawn and other missions before interpreting red spectral slope in ground based spectra of asteroids as an indicator of space weathering.

9. Summary and Conclusions

Ground-based and HST observations of Vesta provided valuable insight into the asteroid's composition, surface albedo and topography prior to the arrival of NASA's Dawn spacecraft. Our comparative study reveals the following:

- Rotation period of Vesta as determined by the Dawn spacecraft (Russell et al., 2012) is 0.222588652 days with an uncertainty of 35 μ s. This is consistent with Drummond et al. (1998) rotational period of 0.22258874 day, the most accurate determination of Vesta's rotational period before Dawn's arrival at Vesta.
- Dawn spacecraft has precisely determined pole orientation of Vesta to be (309.03°, 42.23°) with an uncertainty of 0.01° (Russell et al., 2012). This is a substantial improvement over the best ground/HST based pole position (305.8°, 41.4°) \pm (3.1°, 1.5°) by Li et al. (2010).
- While the Dawn FC lightcurve is much smoother than the HST lightcurve due to much higher signal-to-noise ratio, the overall agreement between the two is excellent in terms of the shape, amplitude, and phase of lightcurves.
- HST topographic map from Thomas, et al (1997) is consistent with Dawn shape model. There are striking similarities between HST topography and the Dawn determined results. HST range of heights was slightly smaller (-12 km to +12 km) than Dawn (-22.45 km to +19.48 km), likely due to much lower spatial resolution of the former, but in general the agreement is very good.
- Global albedo/color maps of Vesta using HST (Binzel et al. 1997; Li et al. 2010) are in excellent agreement with Dawn FC maps (Reddy et al. 2012). East-West

723 hemispherical dichotomy observed in ground-based (e.g., Gaffey 1997) and HST
724 images (Thomas et al. 1997a) has been confirmed by Dawn FC color images.

- 725 • Ground-based telescopic observations indicated the possible presence of a 3- μ m
726 absorption feature. Hasegawa et al. (2003) and Rivkin et al. (2006) suggested
727 contamination from impacting carbonaceous chondrites as possible cause of this
728 feature. Dawn observations of Vesta (De Sanctis et al. 2012b; Prettyman et al.
729 2012; McCord et al. 2012; Reddy et al. 2012b) confirm these ground-based
730 observations.
- 731 • Predominance of diogenite-rich material in the higher albedo Eastern hemisphere
732 observed by ground-based observers (Gaffey 1997; Binzel et al. 1997; Vernazza
733 et al. 2005; Carry et al. 2010; Li et al. 2010) has been confirmed by Dawn (Reddy
734 et al. 2012a).
- 735 • A majority of albedo and color units observed in HST images of Vesta (Binzel et
736 al. 1997; Li et al. 2010) have been confirmed by Dawn FC observations.
- 737 • Dawn data supports an alternative interpretation of “olivine-rich” unit observed
738 by Gaffey (1997). The low BAR for Oppia region, which was interpreted as
739 olivine by Gaffey (1997), would not be so interpreted based on Dawn data (Le
740 Corre et al. (2011).
- 741 • Ground-based observations have severe limitations in identifying space
742 weathering and constraining its magnitude on individual small bodies. Dawn
743 observations have demonstrated that lunar-style space weathering does not
744 operate on Vesta, despite both objects having a basaltic surface composition
745 (Pieters et al. 2012).

- Precursor studies of Vesta have been very successful in accurately characterizing its physical properties. This can be attributed to two factors: a) availability of high quality of ground-based and HST data, and b) interpretations backed by laboratory spectra and studies of samples of HED meteorites

Acknowledgement

We thank the Dawn team for the development, cruise, orbital insertion, and operations of the Dawn spacecraft at Vesta. The Framing Camera project is financially supported by the Max Planck Society and the German Space Agency, DLR. We also thank NASA's Dawn at Vesta Participating Scientist Program for funding the research. A portion of this work was performed at the Jet Propulsion Laboratory, California Institute of Technology, under contract with NASA. Dawn data is archived with the NASA Planetary Data System. VR would like to thank Juan Andreas Sanchez and Guneshwar Singh Thangjam for their help in improving the manuscript.

References

- Archinal, B.A., et al., 2011. Report of the IAU/IAG Working Group on cartographic coordinates and rotational elements: 2009. *Celest. Mech. Dynam. Astron.* 109, 101-135.
- Beck, A.W., McSween, H.Y., Jr., 2010. Diogenites as polymict breccias composed of orthopyroxenite and harzburgite. *Meteorit. Planet. Sci.* 45, 5, 850-872.
- Binzel, R.P., Gaffey, M.J., Thomas, P.T., Zellner, B.H., Storrs, A.D., Wells, E.N., 1997. Geologic mapping of Vesta from 1994 Hubble Space Telescope images. *Icarus* 128, 95-103.
- Bobrovnikoff, N.T., 1929. The spectra of minor planets. *Lick Obs. Bull.* 407, 18-27.
- Buchanan, P.C., Zolensky, M.E., Reid, A.M., 1993. Carbonaceous chondrite clasts in the howardites Bholghati and EET87513. *Meteoritics* 28, 5, 659-669.

Carry, B., Vernazza, P., Dumas, C., Fulchignoni, M., 2010. First disk-resolved spectroscopy of (4) Vesta. *Icarus* 205, 473-482.

Chamberlain, M.A., Lovell, A.J., Sykes, M.V., 2007. Submillimeter lightcurves of Vesta. *Icarus* 192, 448.

Chang, Y.C., and Chang, C.-S., 1962. Photometric investigations of seven variable asteroids. *Acta Astron. Sin.* 10, 101-111.

Cloutis, E.A., Gaffey, M.J., Jackowski, T.L., Reed, K.L., 1986. Calibrations of phase abundance, composition and particle size distribution for olivine-orthopyroxene mixtures from reflectance spectra. *J. Geophys. Res.* 91, 11641-11653.

Cuffey, J., 1953. Pallas, Vesta, Ceres and Victoria; photoelectric photometry. *Astron. J.* 58, 212.

Degewij, J., 1978. Photometry of faint asteroids and satellites. Ph.D. thesis, Leiden Observatory.

Degewij, J., Tedesco, E.F., Zellner, B., 1979. Albedo and color contrasts on asteroid surfaces. *Icarus* 40, 364-374.

De Sanctis, M.C., et al., 2012a. Spectroscopic characterization of mineralogy and its diversity across Vesta. *Science* 336, 697-700.

De Sanctis, M.C., et al., 2012b. Detection of Widespread Hydrated Materials on Vesta by the VIR Imaging Spectrometer On Board the Dawn Mission. *Ap. J. Lett.* 758.

Drummond, J., Christou, J., 2008. Triaxial ellipsoid dimensions and rotational poles of seven asteroids from Lick Observatory adaptive optics images, and of Ceres. *Icarus* 197, 480-496.

Drummond, J., Eckart, A., Hege, E.K., 1988. Speckle interferometry of asteroids. *Icarus* 73, 1-14.

Drummond, J.D., Fugate, R.Q., Christou, J.C., 1998. Full adaptive optics images of asteroids Ceres and Vesta rotational poles and triaxial ellipsoid dimensions. *Icarus* 132, 80-99.

Gaffey, M. J., 1997. Surface lithologic heterogeneity of asteroid 4 Vesta. *Icarus* 127, 130-157.

Gaffey, M.J., 2010. Space weathering and the interpretation of asteroid reflectance spectra. *Icarus* 209, 564-574.

- Gaskell, R. W. and 15 colleagues, 2008. Characterizing and navigating small bodies with imaging data, *Meteoritics and Planetary Science* 43:1049-1062.
- Gaskell, R. W., 2011, Optical Navigation near small bodies AAS paper 11-220, AAS/AIAA Space Flight Mechanics Meeting, New Orleans, LA, 2011.
- Gehrels, T., 1967. Minor planets. I. The rotation of Vesta. *Astro. J.* 72, 929-938.
- Groeneveld, I., Kuiper, G.P., 1954. Photometric studies of asteroids. I. *Astrophys. J.* 120, 200-220.
- Hasegawa, S., Murakawa, K., Ishiguro, M., Nonaka, H., Takato, N., Davis, C.J., Ueno, M., Hiroi, T., 2003. Evidence of hydrated and/or hydroxylated minerals on the surface of asteroid 4 Vesta. *Geophys. Res. Lett.* 30,
- Haupt, H., 1958. Photoelektrisch-photometrische studies an Vesta. *Mitt. Sonnenobs. Kanzelhöhe* 14, 303.
- Herrin, J.S., Zolensky, M.E., Cartwright, J.A., Mittlefehldt, D.W., Ross, D.K., 2011. Carbonaceous chondrite-rich howardites, the potential for hydrous lithologies on the HED parent. *Lunar Planet. Sci. XLII*, 2806 (abstract#1608).
- Hiroi, T., Pieters, C.M., 1998. Origin of vestoids suggested from the space weathering trend in the visible reflectance spectra of HED meteorites and lunar soils. *Antarct. Meteor. Res.* 11, 163-170.
- Le Corre, L., Reddy, V., Nathues, A., Cloutis, E.A., 2011. How to characterize terrains on 4 Vesta using Dawn Framing Camera color bands? *Icarus* 216, 2, 376-386.
- Le Corre, L., et al., 2012. Nature of orange ejecta around Oppia and Octavia craters on Vesta from Dawn Framing Camera. *Meteorit. Planet. Sci. Supplement* 5125 (abstract).
- Li, J.-Y., et al., 2010. Photometric mapping of Asteroid (4) Vesta's southern hemisphere with Hubble Space Telescope. *Icarus* 208, 238-251.
- Li, J.-Y., et al., 2011. Improved measurement of Asteroid (4) Vesta's rotational axis orientation. *Icarus* 211, 528-534.
- Li, J.-Y., et al., 2012. Investigating the origin of bright materials on Vesta: synthesis, conclusions, and implications. *Lunar Planet. Sci. XLIII*, 1659 (abstract).
- Loeffler, M.J., Baragiola, R.A., Murayama, M., 2008. Laboratory simulations of redeposition of impact ejecta on mineral surfaces. *Icarus* 196, 285-292.
- Magnusson, P., 1986. Distribution of spin axes and senses of rotation for 20 large asteroids. *Icarus*, 68, 1-39.

- McCord, et al., 2012. Dark material on Vesta: adding carbonaceous volatile-rich materials to planetary surfaces. *Nature* 491, 83-86.
- Murchie, S., et al., 2002. Color variations on Eros from NEAR multispectral imaging. *Icarus* 155, 145-168.
- Noble, S.K., Keller, L.P., and Pieters, C.M., 2011. Evidence of space weathering in regolith breccias II: Asteroidal regolith breccias. *Meteorit. Planet. Sci.* 45, 2007-2015.
- Pieters, C.M., et al., 2000. Space weathering on airless bodies: Resolving a mystery with lunar samples. *Meteorit. Planet. Sci.* 35, 1101-1107
- Pieters, C.M., et al., 2012. The distinctive space weathering on Vesta. *Nature* 491, 79-82.
- Prettyman, T.H., et al., 2012. Elemental mapping by Dawn reveals exogenic H in Vesta's howarditic regolith. *Science* 338, 6104, 242-246.
- Reddy, V., Gaffey, M.J., Kelley, M.S., Nathues, A., Li, J.-Y., Yarbrough, R., 2010. Compositional heterogeneity of Asteroid 4 Vesta's Southern Hemisphere: Implications for the Dawn Mission. *Icarus* 210, 2, 693-706.
- Reddy, V., et al., 2012a. Albedo and color heterogeneity of Vesta from Dawn. *Science* 336, 700-704.
- Reddy, V., et al., 2012b. Delivery of dark material to Vesta via carbonaceous chondritic impacts. *Icarus* 221, 2, 544-559.
- Reddy, V., et al., 2012c. Photometric, spectral phase and temperature effects on Vesta and HED meteorites: Implications for Dawn mission. *Icarus* 217, 153-168.
- Rivkin, A.S., McFadden, L.A., Binzel, R.P., Sykes, M., 2006. Rotationally-resolved spectroscopy of Vesta I: 2-4 μ m region. *Icarus* 180, 2, 464-472.
- Russell, C.T., et al., 2012. Dawn at Vesta: Testing the protoplanetary paradigm. *Science* 336, 684-686.
- Sanchez, J.A., Reddy, V., Nathues, A., Cloutis, E.A., Mann, P., Hiesinger, H., 2012. Phase reddening on near-Earth asteroids: Implications for mineralogical analysis, space weathering and taxonomic classification. *Icarus* 220, 36-50.
- Schenk, P., et al., 2012. The geologically recent giant impact basins at Vesta's south pole. *Science* 336, 6082, 694-696.

- Seidelmann, P.K., et al., 2002. Report of the IAU/IAG Working Group on cartographic coordinates and rotational elements of the planets and satellites: 2000. *Celest. Mech. Dynam. Astron.* 82, 83-110.
- Seidelmann, P.K., et al., 2005. Report of the IAU/IAG Working Group on cartographic coordinates and rotational elements: 2003. *Celest. Mech. Dynam. Astron.* 91, 203-215.
- Seidelmann, P.K., et al., 2007. Report of the IAU/IAG Working Group on cartographic coordinates and rotational elements: 2006. *Celest. Mech. Dynam. Astron.* 98, 155-180.
- Sierks, H., et al., 2011. The Dawn Framing Camera. *Space Sci. Rev.* 163, 263-327.
- Taylor, R.C., 1973. Minor planets and related objects. XIV. asteroid (4) Vesta. *Astron. J.* 78, 1131-1139.
- Taylor, R.C., Tapia, S., Tedesco, E.F., 1985. The rotation period and pole orientation of asteroid 4 Vesta. *Icarus* 62, 298-304.
- Taylor, L.A., Pieters, C.M., Keller, L.P., Morris, R.V., McKay, D.S., Patchen, A., Wentworth, S., 2001. The effects of space weathering on Apollo 17 mare soils: Petrographic and chemical characterization. *Meteorit. Planet. Sci.* 36, 285-300.
- Thomas, P.C., Binzel, R.P., Gaffey, M.J., Zellner, B.H., Storrs, A.D., Wells, E., 1997a. Vesta: Spin pole, size, and shape from HST images. *Icarus* 128, 88-94.
- Thomas, P.C., et al., 1997b. Impact excavation on asteroid 4 Vesta: Hubble Space Telescope results. *Science* 277, 1492-1495.
- Vernazza, P., Mothé-Diniz, T., Barucci, M.A., Birlan, M., Carvano, J.M., Strazzulla, G., Fulchignoni, M., Migliorini, A., 2005. Analysis of near-IR spectra of 1 Ceres and 4 Vesta, targets of the Dawn mission. *Astron. Astrophys.* 436, 3, 1113-1121.
- Vernazza, P., Brunetto, R., Strazzulla, G., Fulchignoni, M., Rochette, P., Meyer-Vernet, N., Zouganelis, I., 2006. Asteroid colors: a novel tool for magnetic field detection? The case of Vesta. *Astron. Astrophys.* 451, L43-L46.
- Veverka, J., et al., 1996. Ida and Dactyl: Spectral reflectance and color variations. *Icarus* 120, 66-76.
- Zellner, B.H., et al., 1997. Hubble Space Telescope images of asteroid 4 Vesta in 1994. *Icarus* 128, 83-87.
- Zellner, N.E.B., Gibbard, S., de Pater, I., Marchis, F., Gaffey, M.J., 2005. Near-IR imaging of asteroid 4 Vesta. *Icarus* 177, 190-195.

Zolensky, M.E., Weisberg, M.K., Buchanan, P.C., Mittlefehldt, D.W., 1996. Mineralogy of carbonaceous chondrite clasts in HED achondrites and the Moon. *Meteoritics* 31, 518-537.

Table 1. List of FC filters (except clear filter) with their respective band passes width and peak.

Filter name	Wavelength center (μm)	FWHM (μm)
F8	0.438	0.040
F2	0.555	0.043
F7	0.653	0.042
F3	0.749	0.044
F6	0.829	0.036
F4	0.917	0.045
F5	0.965	0.086

Table 2. Observational circumstances for Dawn data collected at Vesta.

Orbital Phase	Best Resolution (meters/pixel)	Sub-Spacecraft Latitude	Distance To Vesta (km)
RC1*	9067	-32°	100,000
RC2	3382	-54°	37,000
RC3	487	-25°	5,200
RC3B	487	-25°	5,200
Survey	252	50° to -90°	2,700
HAMO** (1)	61	66° to -87°	660 to 730
LAMO***	16	85° to -90°	190 to 240
HAMO (2)	60	85° to -85°	640 to 730

*Rotational Characterization

**High Altitude Mapping Orbit

***Low Altitude Mapping Orbit

Table 3. Values for right ascension, declination of the spin pole, ephemeris position of the prime meridian, obliquity, right ascension of vernal equinox, longitude of Olbers Regio, longitude of Claudia and long axis longitude in pre-Dawn coordinate systems (I to VI) and Claudia coordinate system (VII). Obliquity is the angular distance between the orbital and rotational poles and vernal equinox is the descending intersection of Vesta's orbital and its equatorial planes. Note that the IIb values were later used by Seidelmann et al., 2001, Seidelmann et al., 2005 and Seidelmann et al., 2007.

	Source	α_0 (RA of Spin Pole)	δ_0 (Dec. of Spin Pole)	W (Ephemeris Position of Prime Meridian)	Obliquity	Right Ascension of Vernal Equinox	Longitude of Olbers Regio	Longitude of Claudia	Long Axis Longitude
I	Drummond et al., 1988	$335^\circ \pm 4^\circ$	$41^\circ \pm 4^\circ$	$299^\circ + 1617.332776^\circ\text{d}$	36°	84°			0°
IIa	Thomas et al., 1997 (HST 1994)	$308^\circ \pm 10^\circ$	$48^\circ \pm 10^\circ$	$287^\circ + 1617.332776^\circ\text{d}$	22°	54°	0°	145°	330°
IIb	Thomas et al., 1997 (HST 1994 + 1996)	$301^\circ \pm 5^\circ$	$41^\circ \pm 5^\circ$	$292^\circ + 1617.332776^\circ\text{d}$	27°	38°	0°	145°	330°
III	Drummond et al., 1998 (uses pole from IIb)	$301^\circ \pm 5^\circ$	$41^\circ \pm 5^\circ$	$310^\circ + 1617.332485^\circ\text{d}$	27°	38°	350°	135°	0°
IV	Drummond & Christou, 2008	$306^\circ \pm 7^\circ$	$37^\circ \pm 7^\circ$	$304^\circ + 1617.332485^\circ\text{d}$	32°	44°	30°	175°	0°
V	Li et al., 2011	$305.8^\circ \pm 3.1^\circ$	$41.4^\circ \pm 1.5^\circ$	$285.8^\circ + 1617.332776^\circ\text{d}$	27.6°	45.6°	0°	145°	330°
VI	Archinal et al., 2011 (uses pole from V)	$305.8^\circ \pm 3.1^\circ$	$41.4^\circ \pm 1.5^\circ$	$292^\circ + 1617.332776^\circ\text{d}$	27.6°	45.6	354°	139°	324°
VII	Russell et al., 2012	$309.03^\circ \pm 0.01^\circ$	$42.23^\circ \pm 0.01^\circ$	$75.39^\circ + 1617.333122^\circ\text{d}$	27.46°	50.91°	210°	356°	180°

Table 4. The observing geometries of Dawn FC data and HST 2007 data we used to compare the lightcurves of Vesta. The last column lists the difference between sub-solar longitude and sub-observer longitude. A positive value indicates that the morning side is imaged, while a negative value indicates that the afternoon side is imaged.

Data Set	Date	Sub-Solar Latitude	Sub-observer latitude	Phase angle	Lat_sun – Lat_obs
Dawn FC	2011-06-30	-25.7°	-32.2°	26.1°	29.1°
HST 2007	2007-05-14/16	-5.3°	-13.4°	9.5°	-5.4°

Table 5. List of albedo and spectral units identified in HST maps of Vesta and their corresponding IAU approved names from Dawn FC data. A complete list of named features on Vesta from the Dawn mission is available at <http://planetarynames.wr.usgs.gov/Page/VESTA/target>

HST Albedo/Spectral Unit	IAU Approved Feature from Dawn FC Map	Type of Feature	Coordinates (Claudia System)	
			Latitude	Longitude
“Olbers”	Dark ejecta E of Marcia, Calpurnia, Minucia	Albedo unit	-10° to +20°	197° to 215°
#13	Eusebia	Crater	-42.2°	204.2°
#11	Vibidia	Crater	-26.9°	220.1°
Q	Numisia	Crater	-7.0°	247°
Z	Teia	Crater	-3.4°	271°
#15	Oppia	Crater	-8°	309°
#3	Canuleia, Justinia area	Craters	-33.7° to -34.4°	294.5° to 317.9
Y	Feralia	Planitia	+4°	312°
K	Marcia	Crater	+10°	190°
A	Octavia ejecta	Ejecta		
B	Octavia	Crater	-3.3°	147°
#8	Lucaria Tholus	Hill	-13°	104°
#6	Pinaria area	Crater	-29°	32°
#4	Rubria, Occia area	Craters	-7.4° to -15.4°	18.4°
#5	Aquila	Crater	-49.7°	41°
#7	Matronalia Rupes	Scarp	-49.5°	82.7°

Figure Captions

Figure 1. Location of Claudia crater in Vesta's western hemisphere with a close up (b) of Claudia's location southeast of merged craters and a detailed view of Claudia crater itself (c).

Figure 2. Rotational lightcurves as observed by Dawn FC during approach to Vesta and by HST in May 2007. The observing geometries are listed in Table 3. In all three panels, red and orange symbols are measured from Dawn FC images, and green symbols are from HST images. Dawn FC observations and HST observations are arbitrarily shifted to align with each other in magnitude at each wavelength. The top panel shows lightcurves from Dawn FC clear filter (F1, effective wavelength 699 nm) in red and F7 (652 nm) in orange, and from HST WFPC F673N filter (673 nm); middle panel from Dawn FC F8 filter (438 nm) and HST F439W filter (431 nm); and lower panel Dawn FC F5 filter (961 nm) and HST F953N filter (953 nm). All lightcurves are plotted with respect to sub-solar longitude in IAU 'Olbers' coordinate system.

Figure 3. (A) Global topography of Vesta from Hubble imaging data (Thomas, et al, 1997) and from Dawn Framing Camera (B) in IAU 'Olbers' coordinate system. Although the absolute scale ranges from -12 to +12 km in HST data and -22 to +19 km in Dawn data, Vesta's relative topography from HST is consistent with Dawn.

Figure 4. (A) HST map of Vesta in 0.673- μm filter projected in the Thomas et al. (1997a) coordinate system based on observations from 1994, 1996 and 2007 oppositions at a resolution of ~ 50 km/pixel. (B) Dawn FC map of Vesta in 0.75-micron filter from RC1 at a resolution of 9.06 km/pixel with prime meridian similar to Thomas et al. (1997a) coordinate system in Fig. 4a. The pole position ($\alpha_0 = 309.03^\circ \pm 0.01^\circ$, $42.23^\circ \pm 0.01^\circ$) is the updated one from Russell et al. (2012) and hence features in the Dawn FC map are slightly rotated with respect to HST map. Fig. 4c is similar to Fig. 4b but the prime meridian is defined in the Claudia coordinate system (Russell et al. 2012) used by the Dawn science team in all their publications.

Figure 5. Band depth ratio (0.75/0.92 μm) map of Vesta from HST (A) and Dawn (B) showing the intensity of the pyroxene 0.90- μm absorption feature in the Thomas et al. (1997a) coordinate system. Areas in red have deeper pyroxene band and areas in blue have weaker bands. HST and Dawn band depth maps are consistent with each other.

Figure 6. Dawn FC color maps of Vesta using data obtained during the RC3B approach phase of the mission in the Thomas et al. (1997a) coordinate system. (A) Albedo map in 0.75 μm filter, (B) Band depth (0.75/0.92 μm) ratio map with red areas depicting deeper 0.90- μm pyroxene band, and (C) eucrite-diogenite ratio (0.98/0.92 μm) map with red areas indicating more diogenitic material and blue areas more eucritic.

Figure 7. Albedo map of Vesta from HST (A) and Dawn (B) showing corresponding bright features and dark features identified by Binzel et al. (1997) and Li et al. (2010).

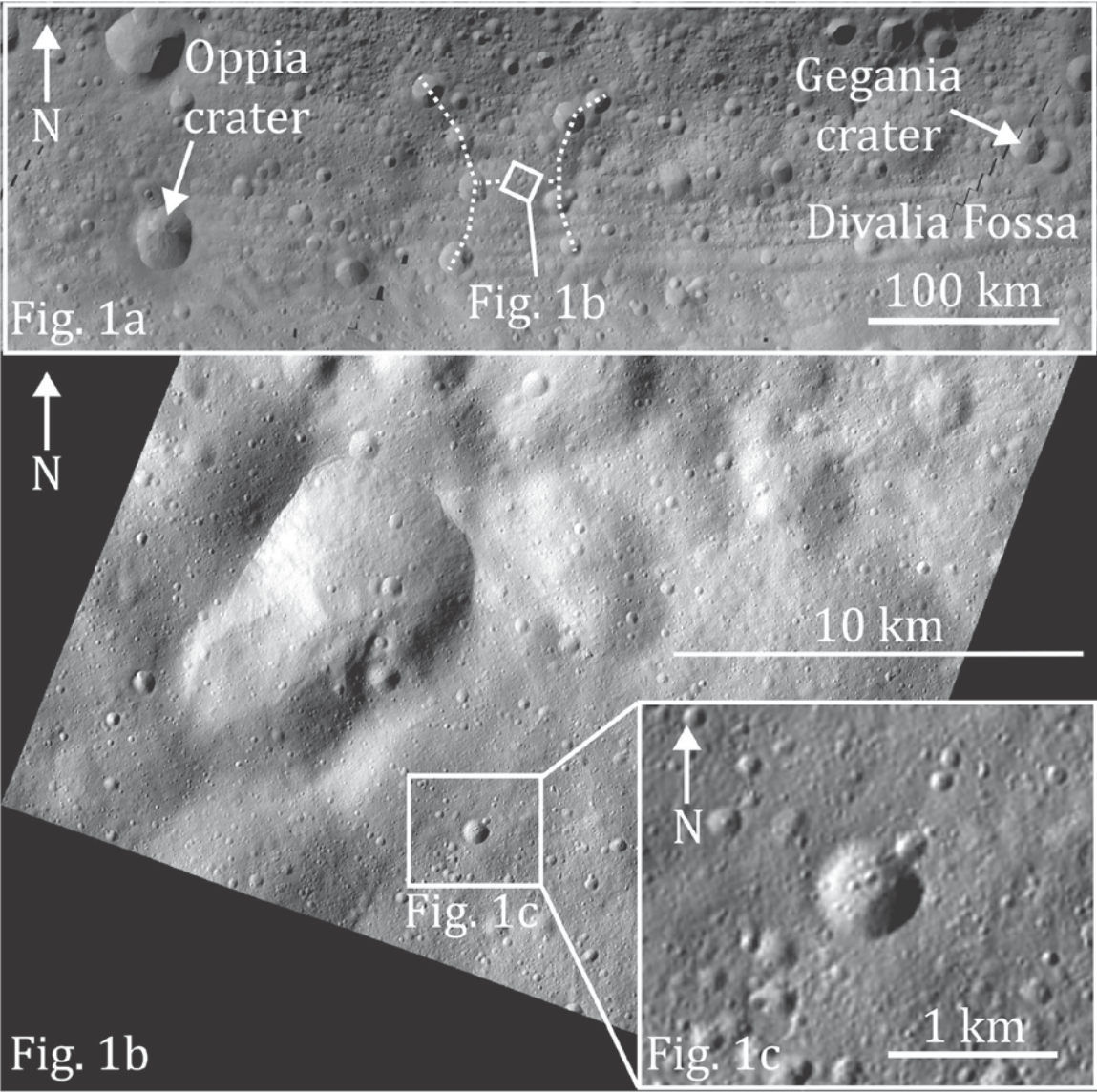
Both maps are in the Thomas et al. (1997a) coordinate system. A global map of Vesta obtained by the Dawn FC camera in Claudia coordinate system is available online at <http://planetarynames.wr.usgs.gov/images/vesta.pdf>

Figure 8. Comparison of compositional units observed in HST map of Vesta from Li et al. (2010) and band depth ratio map from Dawn. Both maps are in the Thomas et al. (1997a) coordinate system.

Figure 9. Comparison of compositional units observed in ground-based map of Vesta from Gaffey (1997) modified by Binzel et al. (1997) and band depth ratio map from Dawn. Both maps are in the Thomas et al. (1997a) coordinate system. Note that this map originally presented in both Gaffey (1997) and modified by Binzel et al. (1997) has wrong latitude due to incorrect calculation of sub-Earth latitude. While the longitudinal location of the compositional units in ground-based maps is well constrained (limited by lightcurve resolution), latitudinal location is weakly constrained as the maps were created using disk integrated data. Due to weak constraints on the latitudinal location of compositional units in Gaffey (1997) and Binzel et al. (1997) maps, comparison with Dawn maps remains valid despite the latitude error.

1095 Figure 1. Dawn, HST, Ground-based Studies of Vesta

1096



1097

1098

1099

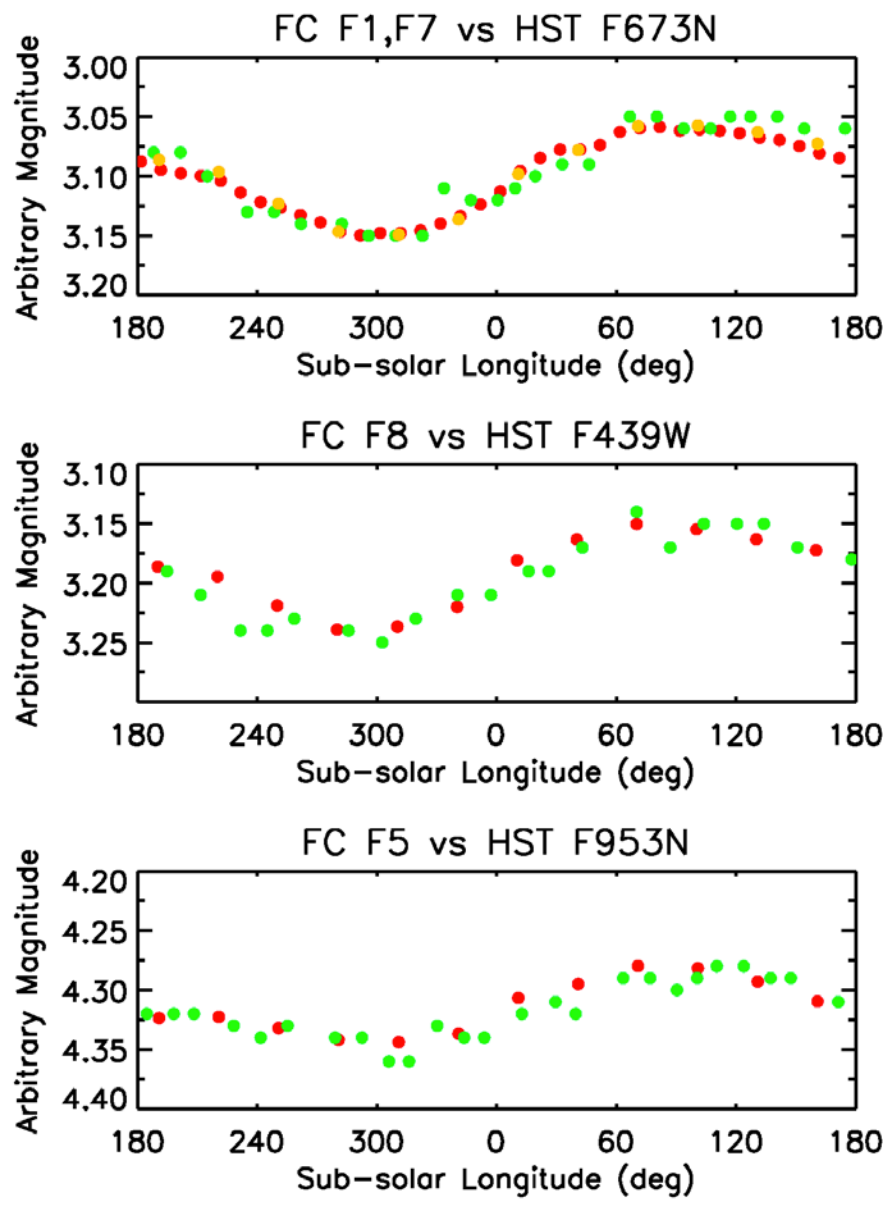
1100

1101

1102

1103 Figure 2. Dawn, HST, Ground-based Studies of Vesta

1104

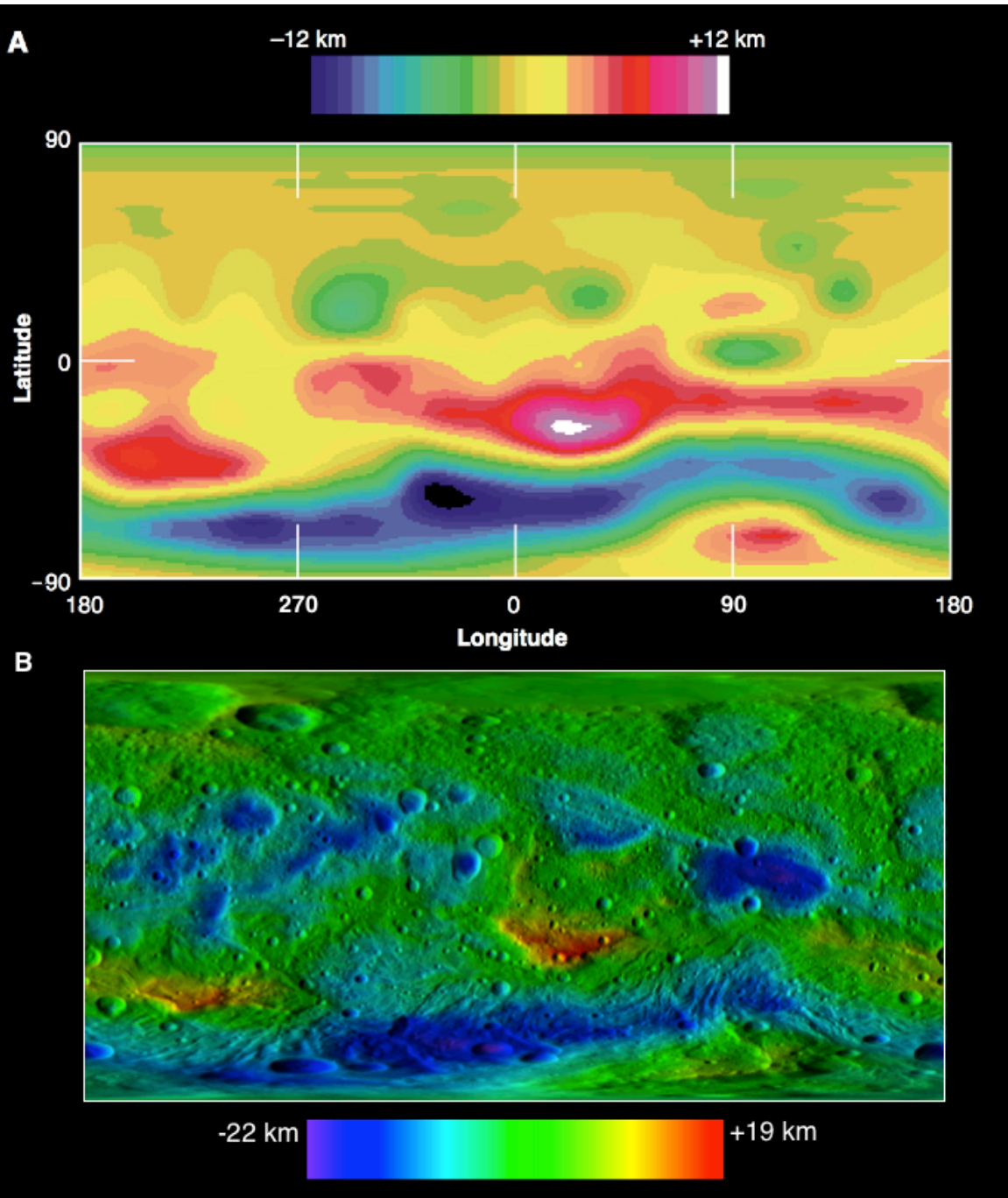


1105

1106

1107 Figure 3. Dawn, HST, Ground-based Studies of Vesta

1108



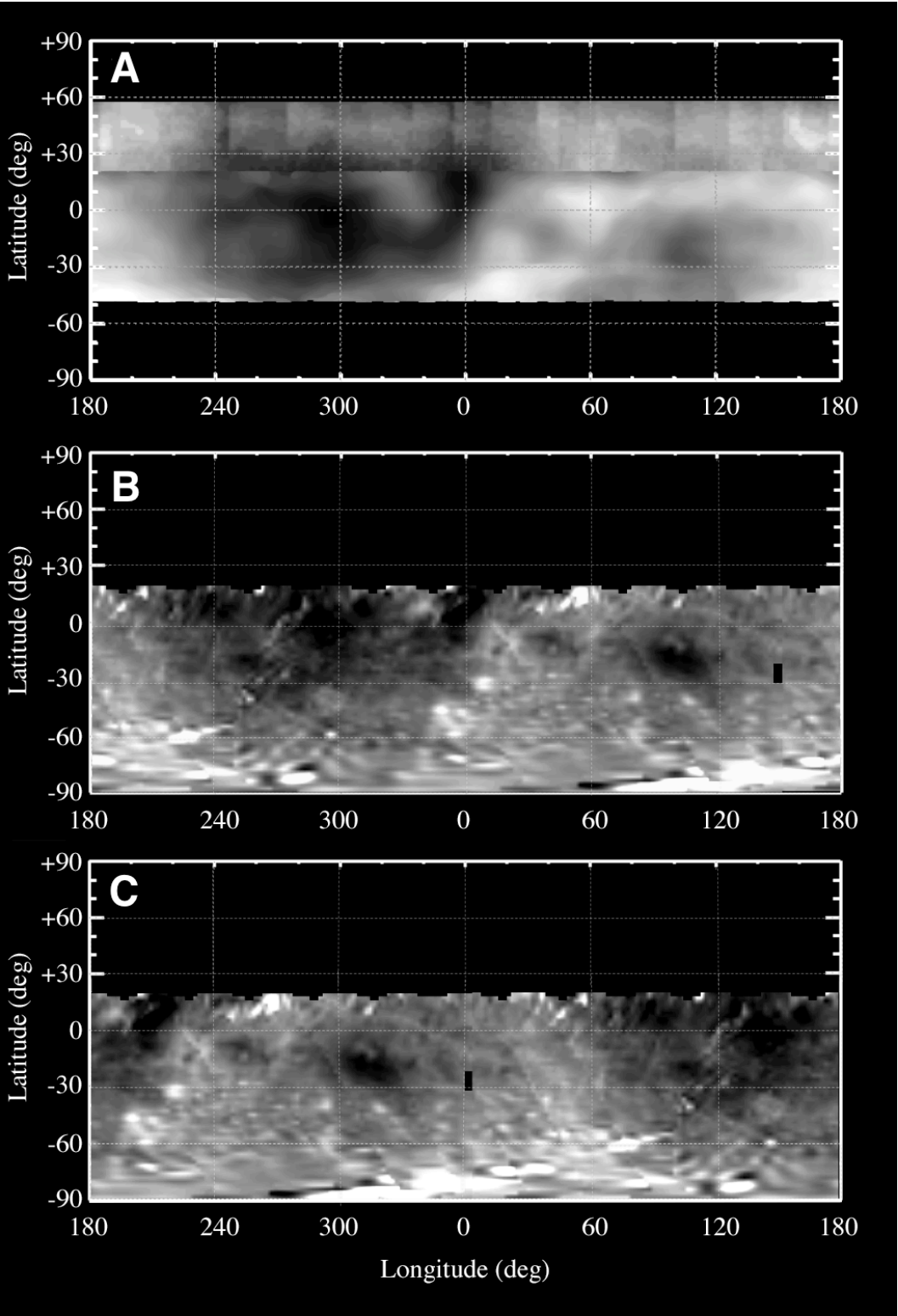
1109

1110

1111

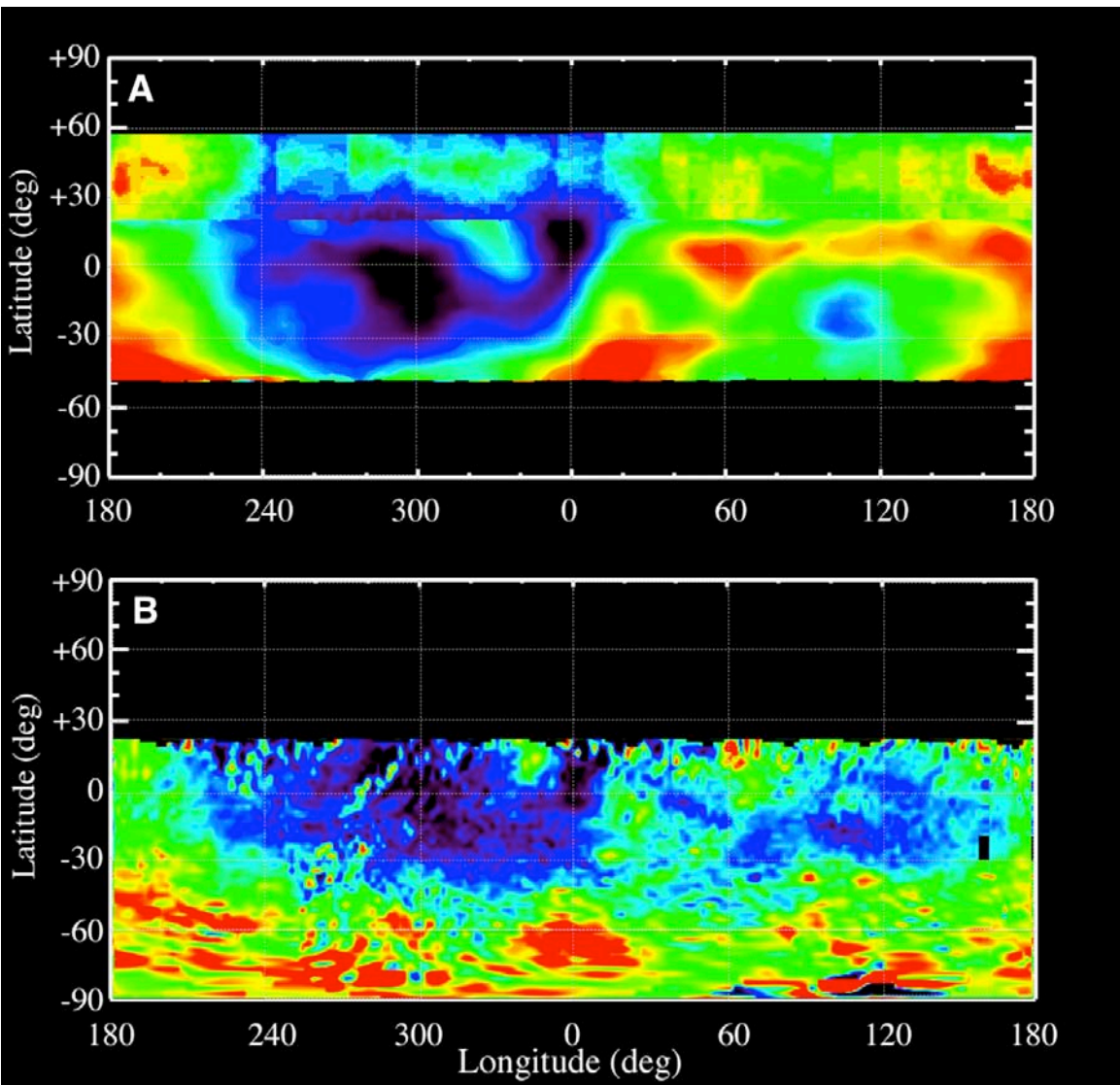
1112 Figure 4. Dawn, HST, Ground-based Studies of Vesta

1113

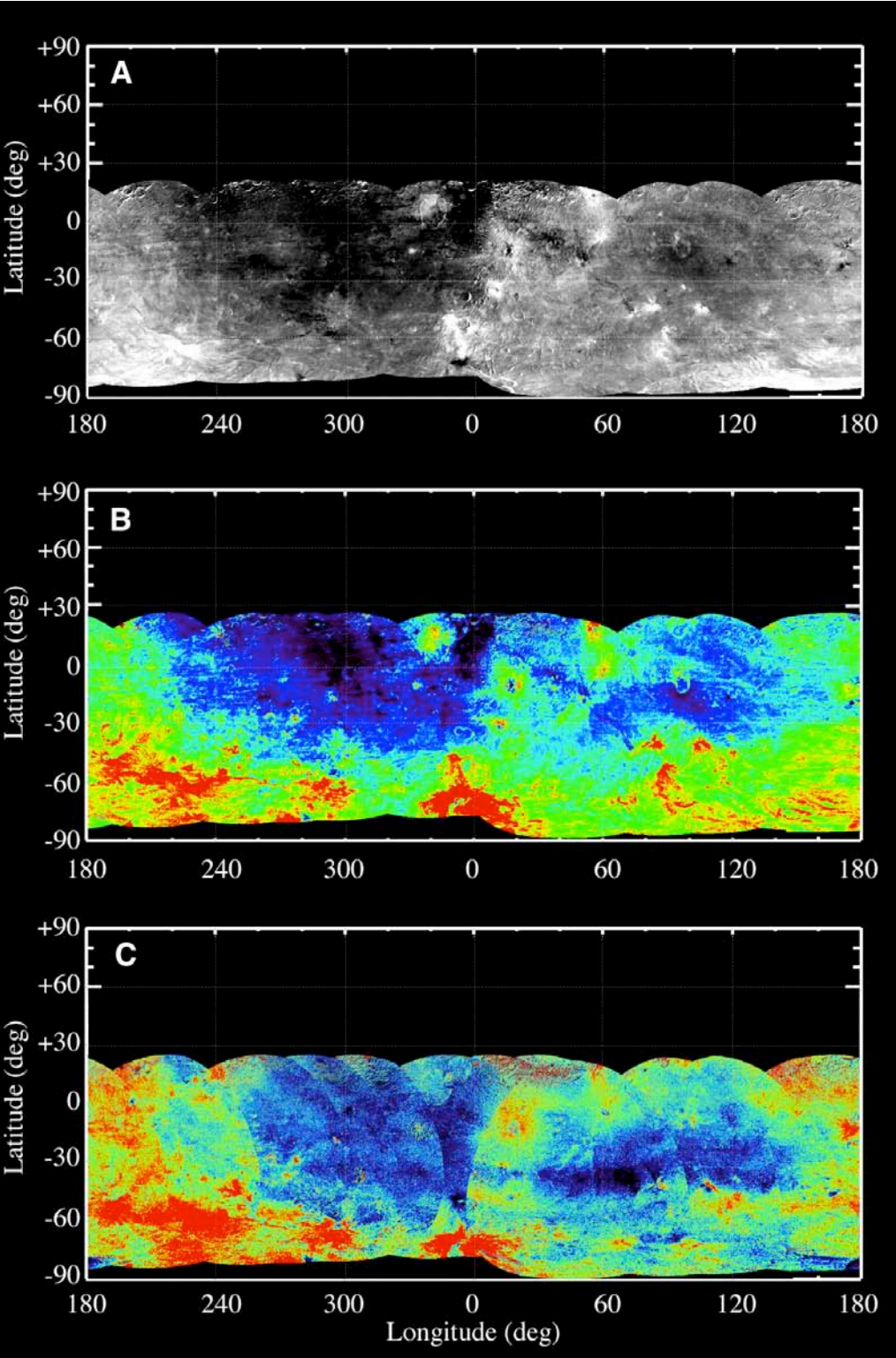


1114

Figure 5. Dawn, HST, Ground-based Studies of Vesta



1124 Figure 6. Dawn, HST, Ground-based Studies of Vesta

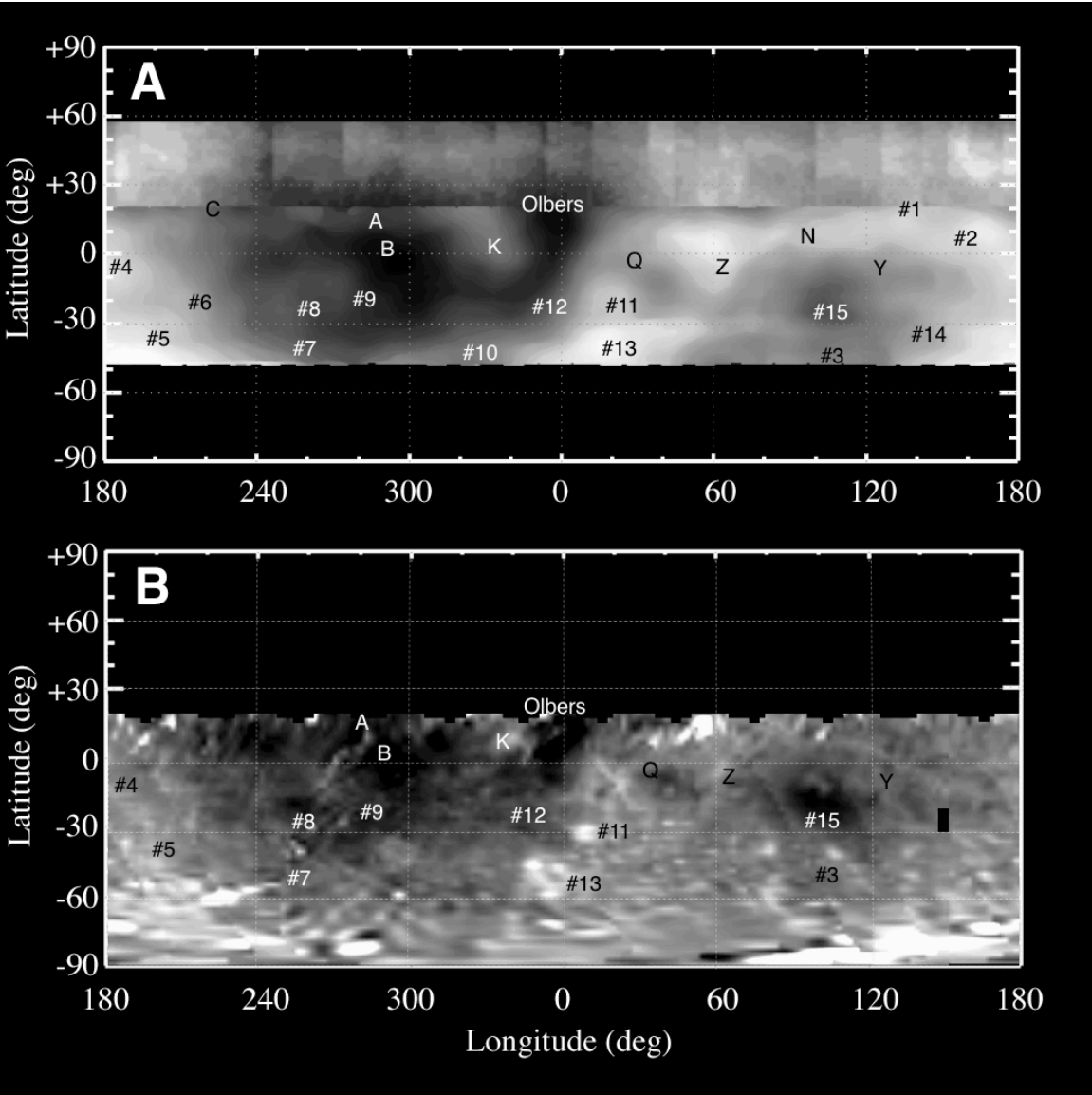


1125

1126

1127 Figure 7. Dawn, HST, Ground-based Studies of Vesta

1128



1129

1130

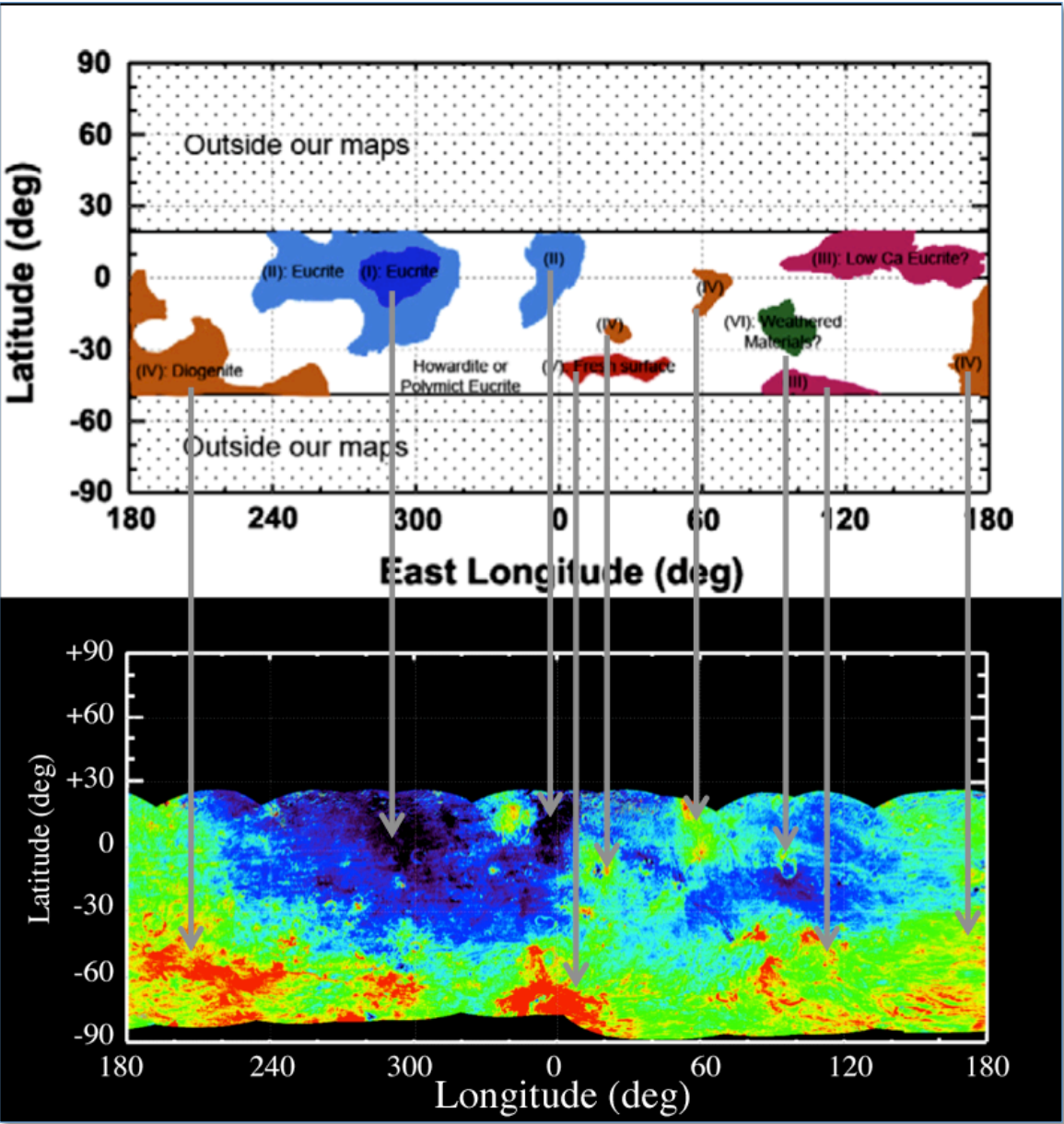
1131

1132

1133

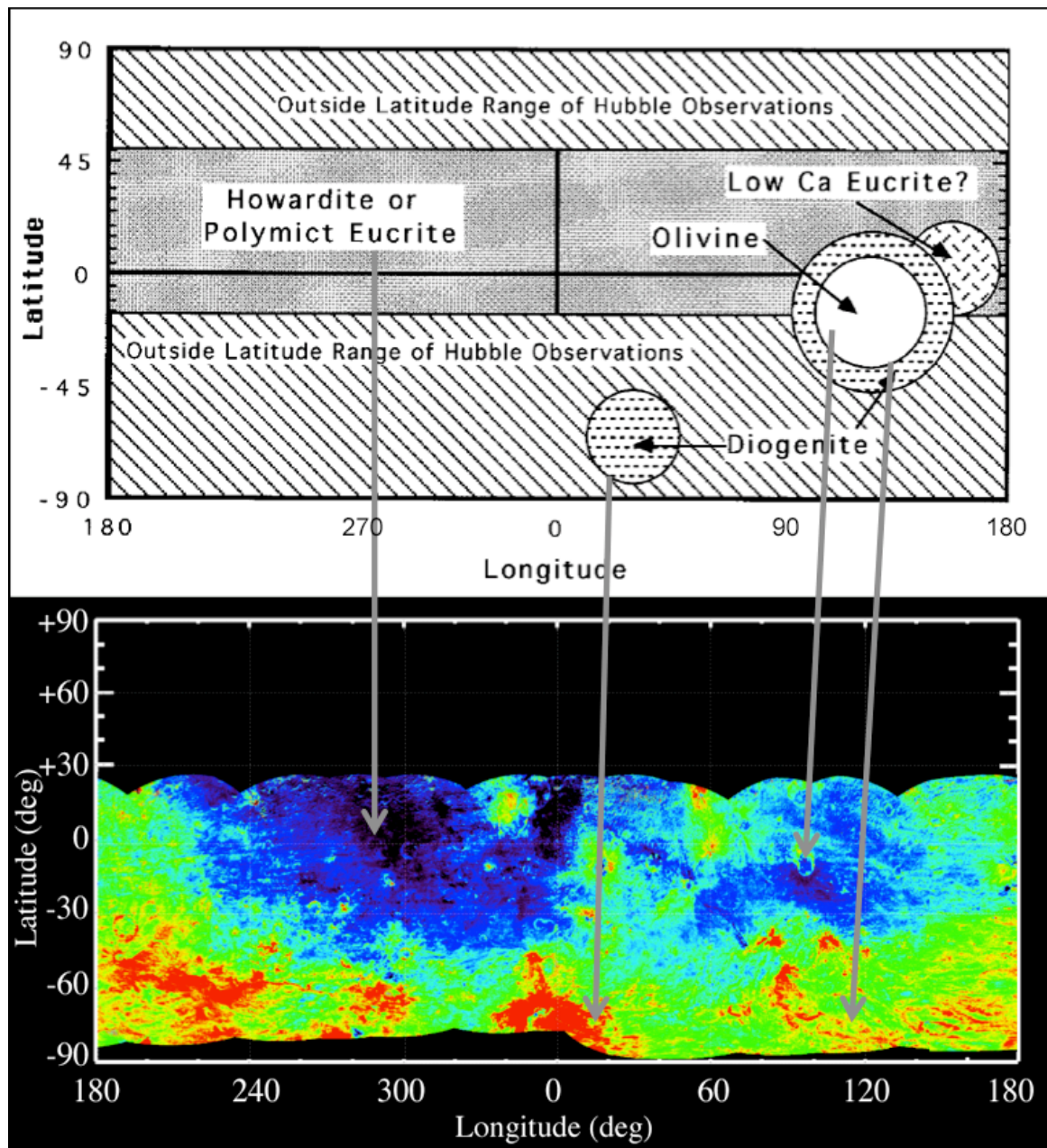
1134

Figure 8. Dawn, HST, Ground-based Studies of Vesta



1142 Figure 9. Dawn, HST, Ground-based Studies of Vesta

1143



1144

1145

1146

1147